Characterization of an Oligocene submarine canyon system and its controlling factors : The La Bonette canyon of the Southern French Alpine Foreland Basin

Louison Mercier, Sébastien Migeon, Jean-Loup Rubino, Jenny Trevisan, Christian Ravenne, Laurent Daghdevirenian, Speranta-Maria Popescu, Mihaela Carmen Melinte-Dobrinescu, Miroslav Bubík

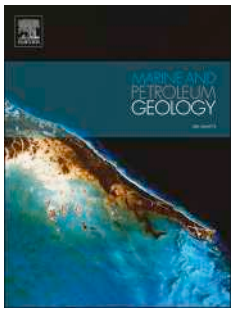

Characterization of an Oligocene submarine canyon system and its controlling factors: The La Bonette canyon of the Southern French Alpine Foreland Basin

Louison Mercier, Sébastien Migeon, Jean-Loup Rubino, Jenny Trevisan, Christian Ravenne, Laurent Daghdevirenian, Speranta-Maria Popescu, Mihaela Carmen Melinte-Dobrinescu, Miroslav Bubík

PII: S0264-8172(24)00057-6

DOI: https://doi.org/10.1016/j.marpetgeo.2024.106745

Reference: JMPG 106745

To appear in: *Marine and Petroleum Geology*

Received Date: 4 September 2023

Revised Date: 30 January 2024

Accepted Date: 1 February 2024

Please cite this article as: Mercier, L., Migeon, Sé., Rubino, J.-L., Trevisan, J., Ravenne, C., Daghdevirenian, L., Popescu, S.-M., Melinte-Dobrinescu, M.C., Bubík, M., Characterization of an Oligocene submarine canyon system and its controlling factors: The La Bonette canyon of the Southern French Alpine Foreland Basin, *Marine and Petroleum Geology* (2024), doi: https://doi.org/10.1016/j.marpetgeo.2024.106745.

Characterization of an Oligocene submarine canyon system and its controlling factors: the La Bonette Canyon of the Southern French Alpine Foreland Basin

Mercier, Louison [a,b]; Migeon, Sébastien [a,c] ; Rubino, Jean-Loup [c] ; Trevisan, Jenny [a] ; Ravenne, Christian [d] ; Daghdevirenian, Laurent [e] ; Popescu, Speranta-Maria [f] ; Melinte-Dobrinescu, Mihaela Carmen [g] ; Bubík, Miroslav [h]

a: Université Côte d'Azur, CNRS, Observatoire de la Côte d'Azur, IRD, Géoazur, 250 rue Albert Einstein, 06560 Valbonne, France

b : PSL University, Mines Paris, Centre de Géosciences, 77305 Fontainebleau Cedex, France

c: Sorbonne University, 75005 Paris, France

d: IFP Energies Nouvelles, 1-4 Av. du Bois Préau, 92852 Rueil-Malmaison, France

e: Watercare Services Limited, 73 Remuera Remuera Rd, Remuera, 1050, New Zealand

f: GeoBiosStratData Consulting, 385 Route du Mas Rillier, 69140 Rillieux-la-Pape, France

g: National Institute of Marine Geology and Geo-Ecology, 23–25 Dimitrie Onciul Street, 70318 Bucharest, Romania

h: Czech Geological Survey, Leitnerova 22, 658 68 Brno, Czech Republic

Corresponding author

Louison Mercier, louison.mercier2@gmail.com

Other authors

Sébastien Migeon, migeon@geoazur.unice.fr

Jean-Loup Rubino, jean-loup.rubino@sorbonne-universite.fr

Jenny Trevisan, trevisan@geoazur.unice.fr

Christian Ravenne, christian.ravenne2@gmail.com

Laurent Daghdevirenian, daghdevirenian.laurent@gmail.com

Speranta-Maria Popescu, geobiostratdata@gmail.com

Mihaela Melinte Dobrinescu, melinte@geoecomar.ro

Miroslav Bubík, miroslav.bubik@geology.cz

Abstract

Submarine canyons are commonly controlled by tectonic structures and, therefore, are key elements of the evolution of convergent margins. The present study focuses on the Southern French Alpine Foreland Basin. Here we use the outcrops of Grès d'Annot Formation and Schistes à Blocs Formation of the Sanguinière-Restefond Sub-basin to study the formation of an ancient canyon in relation to extensive tectonics of the Colombart Structure. The Grès d'Annot Upper Erosion Surface (GAUES) and faults have been mapped in the field and using airborne and drone pictures. Moreover, the planform pattern of the canyon was reconstructed using GIS modelling. Finally, the deposition age of the Schistes à Blocs Formation, which is considered to belong to the Lower Rupelian, has been constrained by the analysis of calcareous nannofossils and benthic foraminifera coming from nine samples. The Colombart Structure is composed of two normal faults of southern vergence bordering a northward dipping rollover anticline, and axially controls the 700 m deep La Bonette Canyon cutting through the underlying Annot Sandstones. The La Bonette Canyon exhibits a succession of sharp erosive features, such as erosive walls, ramps and terraces. The cross-section profile of the La Bonette Canyon exhibits a tectonic control at several scales: it is asymmetric as well as the thalweg is, which is made of an erosive ramp exploiting the underlying structural dip, and an axial incision whose location is controlled by faults. Faults also commonly control smaller scale morphologies, but also the capture of tributaries at right angles with the canyon axis, testifying for a rectangular drainage pattern. The GAUES is interpreted to result from retrogressive erosion and erosion by gravity currents affecting partially lithified turbidites following three main triggering factors which are: i) a possible tilting of the basin towards the west or north-west, and ii) the 3rd order eustatic fall linked to the *Oi1a* $\delta^{18}O$ event, and iii) the increasing erosive power of gravity currents, which were sourced from the remobilized front of the Autapie nappe during its advance in the basin. Tectonic activity and canyon excavation also triggered destabilization of the flanks during deposition of the Schistes à Blocs Formation.

Key words

Submarine canyon, Annot Sandstones Formation, Schistes à Blocs Formation, normal faults, rollover anticline, Alpine foreland Basin, retrogressive erosion, differential lithification

63 **Abbreviations**

64

65 DTM: Digital Terrain Model

66 GAUES: Grès d'Annot Upper Erosion Surface

67 LBC: La Bonette Canyon

68 MTD: Mass transport deposit

69

1. Introduction

Submarine canyons are erosive conduits allowing the transport of particles from the continental shelves to the abyssal plains (Menard, 1955; Normark and Carlson, 2003; Shepard, 1981). They are commonly found on both the passive and active continental margins of most of the world's oceans (Shepard, 1972; Shepard and Dill, 1966; Harris and Whiteway, 2011). Canyon formation and evolution are often the result of multiple processes (Shepard, 1981), which may act simultaneously or alternatively to excavate and to refresh the canyons axis both in downslope and upslope directions (Pratson et al., 1994; Pratson and Coakley, 1996; Shepard, 1981). Eustatic fall has long been considered as the key factor in canyon initiation and evolution (Allin et al., 2017; Baztan et al., 2005; Rasmussen, 1994). However, the formation of some canyons during high sea levels implies the strong impact of other factors such as active tectonism (Fulthorpe et al., 2000; Park et al., 2019) and fault activation (Collot et al., 2019; Ratzov et al., 2012) which could modify locally the slope angle and its orientation and could capture the canyon pathway and the steepness of their flanks. Finally, large collapses related to fault activity and margin deformation may cause a change in direction of the canyons and locally block the downstream transport of particles by damming the canyon axis (Ratzov et al., 2012).

Structural fabric related to faults of various sizes appear to be an important controlling factor on the planform pattern of submarine canyons (Greene et al., 1991). Sharp changes in the orientation of canyon axes, and the capture of tributaries along tectonic structures characterize a rectangular drainage pattern. The latter has long been known on land (Zernitz, 1932) but was recently described for submarine canyons based on 3D seismic data in the Niger Delta (Mercier et al., 2023). The main features of such rectangular submarine drainage pattern of canyons include: (i) abrupt even right-angle changes of orientation of the course of the main canyon and of tributaries, (ii) coalescence of tributaries and (iii) increase of drainage order when crossing one or more fault(s) (Mercier et al., 2023). The growth of anticlinal structures is particularly responsible for the development of canyon branches with a slope opposite to the direction of the regional slope (Di Celma et al., 2016; Mercier et al., 2023). Normal faults can control other canyon properties, such as: (i) the asymmetry of cross-section profile (Almeida et al., 2015; Mercier et al., 2023), and (ii) the location of morphological walls of pluri-decametric height to hectometric height (Mercier et al., 2023).

The present study focuses on new observations and interpretations of the so-called Schistes à Blocs Formation cutting through the Grès d'Annot Formation. The study area is located in the north-eastern part of the Southern French Alpine Foreland Basin, more precisely in the northern part of Sanguinière-Restefond Sub-basin located along the northwestern edge of the Argentera Massif (Fig. 1A). We focus on the mapping and the morphological analysis of the erosive surface which is interposed between the Grès d'Annot Formation below and the Schistes à Blocs Formation above, to propose a robust

interpretation in term of submarine drainage system associated with the formation of canyons. By comparison with present-day submarine canyons, well-documented examples of outcropping ancient canyons are still rare (Anderson et al., 2006; Di Celma, 2011; Di Celma et al., 2014, 2013; Ito et al., 2014; Ito and Saito, 2006; Janocko and Basilici, 2021; Seidler, 2000; Zecchin et al., 2011; Zecchin and Caffau, 2020). The study provides a rare opportunity to, firstly, further improve the criteria for recognising fossil submarine canyons in outcrops and to develop an approach to reconstruct their planform pattern by integrating field observation and measurements together with GIS modelling. Secondly, it allows to better constrain the influence of extensive external factors, such as the tectonics on canyon morphology and evolution. Thirdly, it also constitutes a field example for subsequent exploration in petroleum provinces presenting analogue combination traps, i.e. thick sand-prone beds incised by a mud-filled canyon. Additionally, a new geological model of the area was proposed, providing new ideas for the evolution of the Southern French Alpine Foreland Basin during the Oligocene.

2. Geological setting

The older deposits preserved within the Southern French Alpine Foreland Basin are the Infranummulitic Conglomerates dated from the Paleocene, and are only preserved in local depocentres (Fig. 1B) (Apps et al., 2004; Campredon, 1972; Gupta, 1997; Lickorish and Ford, 1998; Meckel et al., 1996; Pairis, 1971; Ravenne et al., 1987; Schettino and Scotese, 2002). Large scale subsidence reached southeastern France during the Middle Eocene (Ford and Lickorish, 2004), forming an arched flexural basin (Apps et al., 2004; Schettino and Scotese, 2002), coinciding with the early Alpine collision phase described by Schmid *et al.* (1996).

During the Late Eocene, the Mesozoic sedimentary cover of the basin was affected by a regional folding, pluri-deca-kilometric in wavelength, which induced the partitioning of the foreland basin into NW-SE to NNW-SSE oriented synclines (Apps, 1985; Elliott et al., 1985; Jean, 1985; Ravenne et al., 1987). Thus, the first basin was progressively deformed westward (Ford and Lickorish, 2004), into at least four parallel sub-basins, several tens of kilometers in length and few tens of kilometers in width, disconnected one from each other (Ravenne *et al.* 1987; du Fornel *et al.* 2004; Joseph and Lomas 2004; Fig. 1A). At the same time, the continuation of the East Iberian Orogen led to the uplift of the Maures-Estérel and Corsican-Sardinian massifs, which abruptly closed off the southern part of the basin and generated terrigenous inputs within the latter (Ford and Lickorish, 2004; Jean, 1985). During the Eocene-Oligocene transition, sub-basins were successively formed and filled up by the westward Nummulitic Transgression (Sztrákos and du Fornel 2003; Fig. 1A), and by the Grès d'Annot Formation (du Fornel

et al., 2004; Elliott et al., 1985; Jean, 1985; Joseph and Lomas, 2004; Ravenne et al., 1987; Sinclair, 1994).

In each foreland sub-basin, infilling started with the deposition in shallow environments of the Calcaires Nummulitiques Formation, while the following Marnes Bleues Formation constituted slope and bathyal deposits (Ravenne *et al.* 1987; Fig. 1B) recording a dramatic increase of local subsidence rate (Ford et al., 2006; Ford and Lickorish, 2004; Jean, 1985). The Grès d'Annot Formation resulted from the formation of a siliciclastic ramp only fed from the south by fan deltas (Jean 1985; Joseph and Ravenne 2001; du Fornel *et al.* 2004; Joseph and Lomas 2004; Fig. 1A). It is delimited at its base and top by fine-grained facies respectively named Marnes Brunes Inférieures and Marnes Brunes Supérieures, respectively, the latter being preserved only in the Trois Evêchés Sub-basin (Fig. 1) (Etienne et al., 2013; Inglis et al., 1981; Ravenne et al., 1987). In the Sanguinière-Restefond Sub-basin and the Trois Evêchés Sub-basin, three key levels are interbedded within the turbidite infilling (Jean 1985; Ravenne *et al.* 1987; du Fornel 2003; Joseph and Lomas 2004; Fig. 1B).

In the northern part of the basin, the top of the Grès d'Annot Formation is truncated by an erosion surface (Jean et al., 1985; Joseph and Lomas, 2004; Kerckhove, 1969; Ravenne et al., 1987) resulting from the incision of submarine canyons (Jean et al., 1985; Ravenne et al., 1987). The canyons were then infilled by the Schistes à Blocs Formation, which consists of two members: (i) the Schistes Bruns are shales and thin-bedded turbidites overlain by (ii) the olistostromes of the Schistes à Blocs Exotiques (Inglis et al., 1981; Jean, 1985; Kerckhove, 1975). The latter are thrusted by the Autapie Nappe (Fig. 1B) whose emplacement is supposed to occur during the Rupelian considering the azoic character of the Schistes à Blocs Formation (Kerckhove, 1969).

The Sanguinière-Restefond Sub-basin was fed by the Saint-Antonin fan delta (Joseph and Ravenne, 2001) and it was connected downstream with the Trois Evêchés Sub-basin (Jean 1985; Ravenne *et al.* 1987; du Fornel *et al.* 2004; Joseph and Lomas 2004; Fig. 1A). The Sanguinière-Restefond Sub-basin is SE-NW oriented; it is 12-kilometer wide at the southeast and it widens northwestward. This morphology controlled the paleocurrent direction within the 900 m-thick turbidite-lobe successions (Jean et al., 1985), which were emplaced during the Rupelian (NP21 biozone; Sztrákos and du Fornel 2003). Turbidite deposits are affected by N50°E growth faults (Bouroullec et al., 2004). Finally, a pluri-kilometric wide and East-West oriented canyon incised the lobe succession over a depth of about 500 m (Jean et al., 1985). Its orientation resulted from a syn-sedimentary control by N80°E normal faults (Lansigu, 2000).

3. Data and methods

3.1. Field work

A revisited geological map of the Bonette-Restefond area (Fig. 2) is presented in this paper. It is based on i) pre-existing maps (Jean, 1985; Kerckhove et al., 1974; Kerckhove and Monjuvent, 1980; Kerckhove and Thouvenot, 2014; Lansigu, 2000), ii) aerial photographs from the IGN (resolution of 0.20 m) and iii) new observations collected during six field campaigns carried out from 2016 to 2021. The latter are referenced in a Global Mapper© GIS project. Detailed mapping of the erosion surface at the top of the Grès d'Annot Formation (GAUES: Grès d'Annot Upper Erosion Surface) was carried out in many places and geolocalized using a Garmin© GPS. The mapping of the Debrite Key-level 1 has been extended from that proposed by Jean (1985) (Fig. 2). The values measured in the field are: (i) the structural dips and fault planes within the Grès d'Annot Formation, (ii) the paleocurrent directions deduced from cross-stratifications, flute casts and groove marks observed within the Schistes à Blocs Formation and the Grès d'Annot Formation, (iii) the dip and slope angle of the GAUES (Fig. 2). The paleocurrent directions were compiled using Georose©, while the fault planes were compiled using Stereonet©. All the measurements were also geo-referenced using a field GPS, and integrated into the GIS project (Figs. 2, 3A).

3.2. Sampling and biostratigraphic dating within the Schistes à Blocs Formation

New biostratigraphic datings within the Schistes à Blocs Formation were carried out on 9 samples to better constrain the age of incision of the GAUES. Eight samples were taken exclusively from the marly facies at the base of the Schistes Bruns Member; they are numbered Bo15, Bo16, Bo17, Bo23, Bo27, Bo34, Bo37 and Bo40 (Tab. SM1). Additionally sample Bo21 comes from the black marly matrix of debrites which constitute the Schistes à Blocs Member (Tab. SM1). Two groups of organisms were studied: (i) calcareous nannofossils and (ii) planktonic and benthic foraminifera.

The study of calcareous nannofossils was carried out from thin slices, prepared according to the usual techniques and analyzed with a polarizing microscope using a x1200 magnification lens. Preservation of the calcareous nannofossils varies from good to poor. The identification of calcareous nannofossils was done according to Perch-Nielsen (1985).

The study of planktonic and benthic foraminifera was carried out after washing and sieving residues at 50, 150 and 200 µm for the unconsolidated sediments. The residues obtained are poor in foraminifera and sample Bo17 is sterile. A total of 37 planktonic foraminifera belonging to 13 species and 133 benthic foraminifera belonging to 25 species were isolated. They show differences in preservation, caused by different sedimentary environments, diagenesis, and duration of transport to the depositional environment. The identification of foraminifera was done according to the usual nomenclature (Bolli et al., 1994; Cicha et al., 1998; Olsson et al., 1999; Pearson et al., 2006; Petrizzo et al., 2011; Wade et al., 2018).

205

206 **3.3 Reconstruction of the GAUES planform pattern**

207 To better constrain the overall planform geometry of the GAUES, a 3D structural restoration of
208 the GAUES and its paleobathymetry was estimated by restoring two major structural elements, and
209 imposing a regional slope gradient. This was done using the ANUDEM software (Hutchinson et al.,
210 2011) via the ArcGIS Pro 3.1 Topo to Raster tool (Fig. 3B). This tool can calculate a possible
211 topographic DTM (digital terrain model, bathymetric in our case) from typed elevation points, respecting
212 the principle of water flow (with watershed), and limiting depressions. The given points are provided by
213 our surveyed GAUES, in XY location, as they correspond to the canyon floor and more generally the
214 seafloor at that time. Based on both the literature (Bouroullec et al., 2004; Cavailhes et al., 2014, 2013;
215 Kerckhove, 1969; Labaume et al., 2009, 1989; Lansigu, 2000; Tempier, 1979) and our field observation,
216 we took into account the main deformation and burial phases that affected the area to derive their Z
217 location from a present-day 5 m-resolution DTM (RGE ALTI®), as follows:

218 (1) A major North-South normal fault (Bergère Fault) crosses the area (Figs. 2, 3A, 3B): we
219 elevated its western part by 50 m. A N120°E anticlinal fold passing through the Tête du Laup deforms
220 the area (Tempier, 1979); we tilted the east-northern part of the study area by 10° upward, and the west-
221 southern part by 20° upward. In order to have the southern part of the area higher than the norther one
222 as proposed by Jean *et al.* (1985), we imposed a global tilt by 5° downward from a N120°E anticline 10
223 km South-West of the previous syncline.

224 (2) Boundary conditions are also necessary to spatially constrain the model: along the eastern limit
225 set at the longitude of E6°51'18", a line of points (every 20 m) is set with the Sanguinière elevation value.
226 A similar southern limit is set at the latitude of N44°18'8" (Fig. 3B).

227 (3) Finally, we excluded some GAUES points in a small area west of the present-day La Bonette
228 top and added two reconstructed points between the La Bonette and the Caire Brun summits, in order to
229 force the model to detect the northern interfluve of the canyon (Fig. 3B).

230 On the resultant DTM, absolute water depth values are given as a guide only, as we are unable to
231 check their accuracy. These water depth values depend in part on the boundary conditions that have been
232 imposed along the eastern and southern edges of the digital model of the area. However, the proportions
233 between the model and field observations are maintained, with the variations in depth (on the model,
234 Fig. 3B) and elevation (in the field, Tab. 1) between the highest and lowest points being of the same
235 order of magnitude.

236

237 **4. Results**

Within the Sanguinière-Restefond Sub-basin, a first morphological description of the erosion surface at the top of the Grès d'Annot Formation was made by Jean (1985). We have completed it at several observation scales to propose a robust morphological reconstruction of a canyon network and the impact of tectonic structures on its formation and evolution.

4.1. Redefinition of the Colombart Structure

4.1.1. Description

In the study area, one of the major tectonic features is the Colombart Structure (Figs. 2, 3A). It is described as a simple N80°E oriented graben whose activity is thought to be contemporary with the deposition of the Schistes à Blocs Formation (Bouroullec et al., 2004; Lansigu, 2000). New field observations make the interpretation of the Colombart Structure more complex. They include (i) the continuity and accurate location of the faults, (ii) the dip values measured in the Grès d'Annot Formation within the Colombart Structure, but also to the north and south of its axis (Fig. 3A).

The Colombart Structure is about 1.5 km wide in its eastern part, and at least 2 km wide in its western part. Here, F1 and F2 are the two main normal faults, as they have the largest map extension, which is about 6 km (Fig. 3A). They have a southward vergence and they define the northern part of the Colombart Structure, in the form of a hemi-graben a few hundred meters wide. The southern part of the Colombart Structure is affected by normal faults F3-6 of lesser extension (Fig. 3A). F3 and F4 are antithetical to F2 and form a relay structure. Faults F5 and F6 constitute the southernmost part of the Colombart Structure (Fig. 3A). They have a southern vergence, and they disappear in the eastern part of the Colombart Structure (Fig. 3A).

Within the Colombart Structure, dips of the Grès d'Annot strata are mainly NNE to NE. They change locally from one hemi-graben to another one, with variations of about 10-15°. The steepest dips are found in the hemi-graben F3-F4, particularly in its eastern half, which corresponds to the Colombart Structure minimum width (Fig. 3A). The vertical offset of the normal faults is difficult to quantify but it has been estimated at about 120 m in some places where the Debrite Key-level 1 outcrops within some structural blocks, with the cumulative F1-F2 offset of about 200 m (Tab. 1).

4.1.2. Interpretation

The higher dip values located in the F2-F4 graben together with the cumulative F1-F2 offset of about 200 m (Tab. 1) allow a reinterpretation of the Colombart Structure as a system of two main normal faults (F1-F2), with southern vergence, controlling a rollover fold with a northward-oriented forelimb. This structural asymmetry is particularly well-developped along the l'Escuzier Pass outcrop (Figs 4, 5).

4.2. Morphology of the GAUES within the Sanguinière-Restefond Sub-basin

4.2.1. Observation

In the Sanguinière-Restefond Sub-basin, stratigraphic correlations demonstrated that the GAUES cuts several hundred meters deep into the underlying sandstones (Jean et al., 1985). Following a S-N line crossing the Tête de Sanguinière and the Cime de la Bonette (Fig. 2), the shape of the GAUES can be reconstructed using its elevation in relation to the stratigraphic markers Debrite Key Level 1 and Debrite Key Level 2 (Fig. 5). One of the highest points of the GAUES is located at the Tête de Sanguinière, where it truncates the sandstones about 600 m above the Debrite Key Level 1 (Jean 1985; Figs 2, 5 and Tab. 1). Here, the GAUES formed a plateau or a surface gently sloping to the north (Fig. 5). The deepest points of the GAUES are found within the Colombart Structure axis and the F2 hanging wall (Figs 3A, 5), where the GAUES is stratigraphically located just a few tens of meters above the Debrite Key Level 2 (Fig. 4B), or even cut it (Fig. 6B). Toward the north, the GAUES is found about 250 m above the Debrite Key Level 1 (Jean *et al.* 1985; Figs 2-3A and Tab. 1) near the Cime de la Bonette, on the F1 footwall, where it formed another high point (Fig. 5).

Thus, the GAUES exhibited a S-N oriented V-shape and asymmetrical profile (Fig. 5). The lowest point of the GAUES in the Colombart Structure is stratigraphically 740 m deeper than it is at the Tête de Sanguinière (Fig. 5 and Tab. 1B). Consequently, the GAUES deepens by 740 m over a distance of 4 km (on the forelimb of the Colombart Structure), which corresponds to an average slope of 10°. Then between its lowest point and the Cime de la Bonette/Pointe de Chaufrède, the GAUES rises 290 m over a distance of 500 m (Fig. 5 and Tab. 1B), which corresponds to an average slope of 30°. The GAUES thus exhibited a gentler slope angle south of the Colombart Structure and a steeper slope angle north of the latter.

4.2.2. Interpretation

Together with a S-N oriented asymmetrical V-shape profile, the GAUES also exhibits a preferential E-W alignment of its stratigraphic lowest points following the Colombart Structure (Figs 2, 3A). The GAUES can thus be described as an E-W elongated and linear erosive conduit with an asymmetrical transverse V-shape profile. Such a planform pattern is also highlighted by the numerical reconstruction of the physiography of the study area (Fig. 3B), in which the conduit also enlarges from about 1 km to about 3 km to the west, over a distance of about 6 km. The eastern termination of the conduit, as observed on the reconstruction (Fig. 3B), is still speculative due to the lack of field data in this part of the study area. This linear erosive conduit is interpreted as the thalweg of the submarine canyon described by Jean *et al.* (1985), and therefore its position is well controlled by the Colombart Structure as assumed by Lansigu (2000) (Fig. 5). We named this major erosive feature the La Bonette

Canyon (LBC). Both its northern and southern flanks are affected by MTDs (mass transport deposits) and secondary tributaries (Figs 3A, 3B) that will be described in the following sections.

Finally, the lowest stratigraphic point of the GAUES was mapped by Jean (1985) and illustrated in the form of a consequent erosion below the Ventrebrun mountain (Dumont et al., 2011), where it truncates 100 m deeper than the Debrite Key Level 1, although the outcrop is located outside of the canyon axis (Figs 3A, 3B). This suggests an overall deepening of the erosion towards the northwest (Dumont et al., 2011) or to the west, which means the La Bonette Canyon would also deepen to the west, as also revealed by the structural restoration of the GAUES planform pattern (Fig. 3B).

In the following paragraphs, we describe the main architectural elements that compose the La Bonette Canyon, including the lateral flanks, the thalweg and its axial incision, some mass-transport deposits and then some secondary tributaries.

4.3. Lateral flanks of the La Bonette Canyon

Ravenne et al. (1987) described a binary character of the GAUES morphology, which exhibits: (i) sub-perpendicular steps relative to the sandstone stratigraphy, and (ii) sub-parallel flats relative to the underlying stratigraphy. We completed these observations by detailing the multi-scale morphology of the erosion surface, also paying attention to its potential offset by faults.

4.3.1. Erosive features affecting the canyon flanks

Along the E-W incision of the La Bonette Canyon, the GAUES classically exhibits a step-like morphology between its highest and lowest points (Figs 4, 6). At least three main types of architectural elements can be discriminated on a metric to hectometric scale: (i) walls, (ii) ramps and (iii) terraces (Fig. 8), giving the GAUES an irregular and crenulated topography. Walls are defined where the GAUES cut through the Annot Sandstones deposits at steep angles varying between 60 and 90° (Fig. 8). They can be metric to pluri-decametric in height depending on whether they affect a single sandstone bed or multiple beds within a stratigraphic unit (Figs 8C, 8D, 8F). The typical height of walls is more frequently multi-metric, resulting from the incision of massive beds separated by thinner shaly levels (Fig. 8C). Sub-vertical walls have masses of deformed Annot Sandstones in contact with the erosive surface or at their base, suggesting they were affected by destabilization processes. The latter could correspond to either limited remobilization of Annot Sandstones following the dip of the erosion surface generating *in-situ* slumps (Fig. 8C), or even the larger destabilization of Annot Sandstones resulting in resedimented strongly-deformed masses packed within the Schistes Bruns Member (Fig. 7C). Like walls, erosive ramps may truncate a single sandstone bed or thicker units, but they exhibit low-value slopes with dips commonly measured close to 10-20° (Figs 8E, 8F) and at the most 40-45° (Fig. 6B). No failure-related

masses of Annot Sandstones are observed at their contact. Both walls and ramps are separated by flatter areas that are sub-parallel to strictly parallel to the Annot Sandstones stratigraphy (Figs 4, 6, 7, 8). They are interpreted as erosive terraces.

Similar morphologies are observed on a centimetric to decimetric scale (Figs 8A, 8B), giving also the GAUES an irregular and crenulated topography at the smallest scale. The latter can exhibit locally superficial crusts of Fe-Mn hydroxides (Fig. 8D). Similar observation were previously used in the Grès d'Annot Formation as an argument in favour of the formation of an erosive surface in a relative deep marine environment (Ravenne et al., 1987).

4.3.2. Location and morphology of the erosive features

Walls and ramps are observed along the whole outcropping segment of the La Bonette Canyon but they are found associated with three different configurations:

1) they affected and eroded the Annot Sandstones without clear evidence of tectonic structures to guide them (Fig. 8C),

2) they formed above faults that affected the Annot Sandstones but that were already inactive by the time of formation of the walls (i.e. fault F0B, Fig. 4B),

3) they formed above syn-sedimentary faults affecting the Annot Sandstones (Figs 4, 6, 7A-B, 9B, 10A).

In configuration 1, unitary walls are up to 60 m high, they exhibit various slope angles ranging from 60° to 90° (Fig. 8F), and in some cases they can be spatially juxtaposed forming up to 90 m high composite walls (Fig. 8E). Along a single canyon flank, several walls are always superimposed and separated by flat terraces of varying widths (Fig. 8E). The latter coincide with shalier intervals.

In configurations 2 and 3, erosive walls are sharp and linear in shape. They are 10 to 100 m high with slope angles greater than 60-70°. Walls are the direct vertical continuity of fault planes, but they can exhibit either the same dip direction and slope angle (as observed at the Colombart Pass for F2 and F3, Figs 6, 7), or a different dip direction and slope value (as in the southern part of Tête Ronde outcrop where F1, which is almost vertical, and with a vertical offset close to 100 m is cut by a wall 40-m high and inclined at 60 to 70°, Figs 3A, 6B). They truncate the footwall and/or the hanging wall of faults, but the associated downslope terraces are commonly located on the hanging wall (Figs. 4 and 6). Note that as for F1 along the Escuzier outcrop (Fig. 4B), most of wall-terrace pairs are undoubtedly sealed by the onlap of the Schistes à Blocs Formation (Figs 7A, 7B).

The impact of the vertical displacement of faults on the height of walls can be questioned, and it does not appear to be a simple linear relationship. In the configuration 2, F0B was the most significant fault, with a N95°E-70°N orientation and a vertical offset of 40 to 45 m (Pochat and Van Den Driessche,

2007). A 40 m-high erosive wall cut through its footwall, but not through the hanging wall (Figs. 3A, 4). In the configuration 3, on the Colombart Pass outcrop, an erosive wall up to 100 m high is located directly in the vertical continuity of the F1b plane, and its height is 30 to 100 times greater than the vertical offset of F1b (Figs 6, 7A). F1e also exhibits a much smaller vertical offset than the height of its associated scarp. The latter is 12-m high whereas the vertical offset of the fault is metric. (Fig. 7B). F1e footwall is truncated by a 60° dipping erosive ramp, and its hanging wall is cut by a wall, which is sealed by the onlap of the Schistes Bruns Member (Figs 6, 7B). The relationship between the height of the wall and the vertical offset of the faults is thus still unclear, particularly considering syn-sedimentary faults active by the time of formation of the GAUES. It suggests that the walls are not only tectonic in origin since they can be guided or not by faults and their height is not strictly controlled by the fault displacement.

4.3.3. Overall architecture of the LBC flanks

The identification of multi-scale erosive features allowed to better describe the flanks of the La Bonette Canyon and to clarify the asymmetry of the transverse profile of the La Bonette Canyon observed at the sub-basin scale (Fig. 5).

The northern flank of the La Bonette Canyon shows a steep geometry on each transverse panorama (Figs 4, 6, 9). It consists of a succession of (i) walls several tens- to a hundred meters-high, separating (ii) narrow erosive terraces. This organization is best observed along the Colombart outcrop, where walls are supported by normal faults (Figs 6, 7A, 7B). A similar configuration is observable along the l'Escuzier Pass (Fig. 4) and the Tête de Glaudon (Fig. 9) outcrops.

The southern flank of the La Bonette Canyon also consists of erosive terraces and walls, but also of erosive ramps. Some preserved erosive ramps are observable at the Escuzier outcrop, where there are two decametric- to pluridecametric-high, the topographically lowest one being located more precisely within the thalweg sensu stricto (Fig. 4B). The erosive ramp which is located on the southern flank sensu stricto is less well preserved, because it crops out along only ten meters and it is intersected by the present-day topography at its southern edge (Fig. 4B). These two features show a very low angle of intersection through the underlying sandstone beds and are even locally sub-parallel to the structural dip, which ranges from 20 to 30° (Fig. 4B).

Thus, the southern flank is generally gentler in slope (Tab. 1A) and wider than the northern flank (Fig. 3B) due to the presence of few ramps that use the structural dip of the rollover (Fig. 4B), whereas the northern flank is steeper and narrower (Figs 3B and 5) due to the presence of walls and narrow terraces only (Fig. 6B).

4.4. The LBC thalweg and its controlling factors

The La Bonette Canyon presents the most representative features of its thalweg along the l'Escuzier Pass outcrop (Fig. 4). Here, the thalweg can be seen along a transverse profile. The thalweg is about 420-m wide and it is delimited by two sub-vertical erosive walls which are several decameters high, the latter being associated with faults F2 and F3 (Fig. 4). Within the thalweg, the axial incision 50-m deep and 220-m wide is also asymmetrical. It is much steeper to the north where it lies against the erosive wall controlled by F2 while a southern gentler ramp constitutes the transition up to the base of the steep wall guided by F3. The slope of the ramp is close to the dip of the underlying Grès d'Annot Formation (Fig. 4). Along the Colombart Pass outcrop (Fig. 6), another example of the thalweg asymmetry can be observed but reversed compared to the previous one. The thalweg is still delimitated by faults F2 and F3 but the 20 m-deep and 170 m-wide axial incision is located against the steep southern wall guided by the fault F3 while a northern gentler ramp gradually intersects the underlying stratigraphy up to the steep wall guided by F2 (Fig. 6).

Thus, the thalweg shows an asymmetrical transverse profile along the La Bonette Canyon, but the orientation of the asymmetry changes depending on the position of the axial incision against fault F2 or fault F3 (Figs. 4 and 6). This shift in the position of the axial incision could suggest syn-sedimentary activity of faults F2 and F3, or alternatively meandering processes of thalweg incision.

4.5. Mass-transport deposits

In the study area, six units consisting of strong soft and brittle deformations bounded by shear planes (Figs 3A, 6, 9, 10, 11C, 11D) are found in contact with the GAUES, in the underlying Annot Sandstones and/or the overlying Schistes Bruns Member. These six deformed units cannot be laterally correlated with the surrounding deposits and they are interpreted as mass transport deposits (MTDs) similar to those found in other contexts (Alves and Lourenço, 2010; Odonne et al., 2011; Sobiesiak et al., 2016). MTDs 1, 2, 4 and 5 are up to 100 m thick and are all located on the Colombart Structure rollover (Figs 3A, 5), MTD3 is located against F2 within the axial incision and MTD6 is located on F1 footwall (Fig. 3A).

MTD1 used faults F2 and F3 as sidewalls (Fig. 6B). It consists of at least three structural blocks whose series cannot be correlated with each other because of their bounding shear zones which are strictly parallel to F2 and F3 (Figs. 3A, 6B). Their folded deformations are oriented to the west. MTD2 followed F4 along its southern edge while its northern edge truncates F3 and laterally thrusts the Schistes Bruns Member (Figs 6B, 7D). MTD2 shows internal reverse faults which delimitate Annot Sandstones packages of different structural dips (Fig. 6B). MTD2 is also associated with failures of Annot Sandstones redeposited within the Schistes Bruns Member near its northern sidewall (Figs 6B, 7C).

MTD3 is a decametric thick and long olistolith which crops out on the eastern side of l'Escuzier Pass (Fig. 3A).

MTD4 and MTD5 are the largest MTDs with dimensions of the order of a kilometre (Figs 3A, 9, 10). They consist of two clearly distinct zones with similar lengths: (i) an extension zone characterized by several successive tilted blocks of Annot Sandstones separated by normal faults (Figs 12a, 12B), and (ii) a compression zone characterized by the superposition of deformed units bounded by thrust faults (Figs 9, 10, 11E, 11F) but also showing juxtaposed internal masses bounded by longitudinal shear zones (Figs 9B, 11C, 11D). In the extension zone, the dip of the faults decreases gradually downstreamward while the dip of the tilted Annot Sandstones increases (Fig. 10). The faults are rooted and stop on a basal decollement surface (Figs 9, 10). Such a MTD architecture is similar to observations made by Frey Martinez *et al.* (2005) on 3D seismic data. Both the frontal parts of MTD4 and MTD5 are roughly oriented northward and their respective frontal ramp thrusts the Schistes Bruns Member (Figs. 9, 10, 11F). The frontal part of MTD4 also exhibits many solitary blocks that were transported northward and packed within the Schistes Bruns Member: it constitutes a mixing zone that reworked the infilling of the La Bonette Canyon thalweg (Fig. 9B).

MTD6 comprises two masses of Annot Sandstones, which are about 10 m thick and 100 m-long. They are located at the eastern and southern sides of Cime de la Bonette and associated with a few tens of meters high wall located at the eastern side of the same mountain (Figs 3A, 3B).

Placed in their environmental context (Fig. 3B), MTD6 affected the northern flank of the La Bonette Canyon close to the interfluve, MTD1 is found within its central thalweg, MTD2, MTD3, MTD4, and MTD5 affected its southern flank at different location above the thalweg floor. Their directions of displacement were defined perpendicular to the strike direction of their internal normal and reverse faults and parallel to their internal longitudinal shear zones (Fig. 11). Transport directions are consistent with the local slope as obtained on the structural reconstruction of the GAUES planform pattern (Fig. 3B). The triggering of these MTDs would be thus closely connected with the formation of the La Bonette Canyon.

4.6. Secondary lateral tributaries

Along the flanks of the LBC thalweg, smaller-scale erosive surfaces can be observed on several transverse outcrops (Figs 3A, 12A). They are V-shaped in cross-section, tens to a hundred meters-deep and a hundred to few hundred meters-wide. In the field, they can be followed for distances of 1 to 2 km, and they are characterized by elongated cartographical depressions (Fig. 3A). They are oriented from ENE-WSW to NNE-SSW, and, therefore, they are sub-parallel to sub-perpendicular to the La Bonette Canyon (Figs 3A, 3B). These features are interpreted as secondary tributaries merging laterally with the

La Bonette Canyon. Five of them are located on the northern side of the La Bonette Canyon, while only one is preserved on the Colombart roll-over (Fig. 3A). As for the LBC flanks, tributaries are formed by a succession of walls, terraces and erosive ramps (Fig. 12A).

The larger tributary is located at L'Alpe outcrop (Fig. 3A). It is a 1-km wide cartographic re-entrant, which intersects the base of the GA Fm. in its western edge, and the Debrite Key Level 2 in its northern part (Fig. 3A). Therefore, it is sub-perpendicular to the La Bonette Canyon (Fig. 3B) and it deepens toward the latter, with a confluence area which would be located in the vicinity of F2 (Fig. 3A).

The opposite orientation is observed for the Baisse de la Plate tributary, because the orientation of its preserved part is NNE-SSW (Fig. 3A). It is 60 m deep and 500 m wide (Fig. 12A). Its V-shape thalweg is bounded by decametric-high walls, the northern one being controlled by F6 (Fig. 12A) which explains the orientation of the tributary fill (Fig. 3A). Some slide blocks of Annot Sandstones are found within the tributary fill, packed within the Schistes Bruns (Fig 12A). The observation of larger volume of slide blocks in its eastern part (Figs 12B, 12C), and its deepening towards the east (Fig. 3A) suggest its orientation follows this direction, i.e. opposite to the orientation of the La Bonette Canyon (Fig. 3B).

4.7. Biostratigraphic dating of the Schistes à Blocs Formation

Within the Sanguinière Restefond Sub-basin, the uppermost levels of the Annot Sandstones have been dated at the end of the NP21 biozone (Sztrákos and du Fornel, 2003). Seven of the eight samples that were collected within the Schistes Bruns yielded marine microfossils, except sample Bo17. The sample Bo21 from the Schistes à Blocs Exotiques Member also yielded marine microfossils. Details of these results are provided in Supplementary Material (Tab. SM1): samples Bo15, Bo16, Bo27, Bo37 and Bo21 included both planktonic and benthic foraminifera and calcareous nannofossils; sample Bo23 contained very few planktonic foraminifera but diversified calcareous nannoplankton; sample Bo34 was very poor with only one significant planktonic foraminifer species; sample Bo39 only displayed a diversified calcareous nannoflora. Figure 13 displays interpreted biostratigraphic calibration of the samples according to foraminifera and calcareous nannofossils (Tab. SM1). Based on these observations, the most suitable age for the Schistes Bruns and Schistes à Blocs Exotiques members would be the interval showing the youngest reliable assemblages for both the foraminifera and nannofossil species. This reasoning results in proposing an early Rupelian age for these members, more precisely including the O1 and O2 foraminifera zones and the NP22-lower NP23 nannoplankton zones (Fig. 13).

5. Discussion

Based on the results previously presented, we first discuss below how external factors triggered the canyon formation and which sedimentary process is mainly responsible for the canyon excavation

during the Rupelian. Finally, we discuss which processes acted at different scales and are involved in the geomorphological control of the La Bonette Canyon.

5.1. Origin of the GAUES

The initiation of submarine canyons is classically correlated with tectonically-related degradation of continental margins (Clayton and Olariu, 2022; Collot et al., 2019; Jackson et al., 2021; Ratzov et al., 2012), or with eustatic falls causing an increasing supply of particles to the continental slope and an increasing triggering of gravity processes at the upper continental slope (Baztan et al., 2005; Mauffrey et al., 2017, 2015; Posamentier et al., 1991; Shepard, 1981), or with a complex balance between tectonics and eustatism (Bourget et al., 2011; Park et al., 2019). We discuss in the following section which external factors triggered the GAUES, and therefore which sedimentary process was mainly responsible for the LBC excavation.

5.1.1. Impact of regional and local tectonics

In order to discuss the regional and/or local role of tectonics in the formation of the Grès d'Annot Upper Erosion Surface, it is first necessary to briefly recall the tectono-sedimentary context in which the GAUES was formed. The GAUES was identified only in the north-western part of the basin (Inglis et al., 1981; Jean et al., 1985; Kerckhove et al., 1974; Kerckhove and Monjuvent, 1980; Kerckhove and Thouvenot, 2014; Ravenne et al., 1987), i.e. within the Sanguinière-Restefond, Trois Evêchés, Lauzanier and Eastern Champsaur sub-basins (Fig. 1A), whereas the Annot Sandstones that deposited in older and more internal sub-basins (i.e. Ventimiglia and Peira Cava sub-basins, Fig. 1A) does not exhibit any erosion surface at its top, and the Schistes à Blocs Formation is consequently concordant there (Lanteaume, 1968; Lanteaume et al., 1990; Perotti et al., 2012; Wazi et al., 1985).

In the study area, the GAUES affected lobe deposits of the Grès d'Annot Formation that thus previously were deposited in a S-N oriented more or less horizontal flat-floored basin. As such, incision of the GAUES required the initiation of a regional slope, which is thought to result from a deformation phase occurring during the Lower Oligocene and possibly only affecting the north-western part of the basin. This deformation phase was not yet described by previous works in this part of the basin, but we suppose that it occurred several times after the deposition of the Annot Sandstones (i.e. during biozones NP22-lower NP23, Fig. 13) and would have favoured the submarine destabilization of the Annot Sandstones.

Secondly, whatever their origin, submarine canyons are often guided or controlled by tectonic structures on convergent margins (Bourget et al., 2011; Han et al., 2017; Micallef et al., 2014; Mountjoy et al., 2009; Ratzov et al., 2012; Soulet et al., 2016). Consequently, the orientations of erosive conduits

544 of the GAUES within all sub-basins must be compared, in order to identify potential differences of slope
545 orientation resulting from local deformation. In the Trois Evêchés Sub-basin, the GAUES is described
546 as 100 m-deep erosive conduits filled-up by the Schistes à Blocs Formation, and whose axes are NNE-
547 SSW oriented (Ravenne et al., 1987), i.e. the same orientation than the general trend of the GAUES in
548 the Sanguinière-Restefond Sub-basin. In the Lauzanier Sub-basin, the GAUES also consists of 100-m
549 deep erosive conduits with a transverse profile deepening along an E-W direction (Mulder et al., 2010),
550 which means the Lauzanier conduits are roughly S-N oriented (Fig. 15). Thus, they are possibly
551 influenced by a slope which is oriented in a direction that is close to the one existing in the Sanguinière-
552 Restefond Sub-basin, i.e. toward the northwest (Fig. 15).

553 As such, there is no clear difference in the orientation of the submarine slope existing within these
554 sub-basins during the formation of the GAUES. The slope remained in the same orientation as the one
555 prevailing during the deposition of the Annot Sandstones, i.e. toward the north-west (du Fornel et al.,
556 2004; Jean et al., 1985; Vinnels et al., 2010). This means that regional deformation would have preserved
557 the polarity of the basin as it was during its infilling by the Annot Sandstones, only increasing the
558 existing slope gradient.

559

560 ***5.1.2. Glacio-eustatic forcing***

561 The question of the nature of the event responsible for the formation of the GAUES must also
562 consider the climatic aspect, since eustatic falls leading to an increasing gravity-flow activity commonly
563 trigger the formation of submarine canyons (Baztan et al., 2005; Galloway et al., 1991; Vail et al., 1991).

564 Studies on the long-term stable New Jersey margin show that since the Late Eocene, sequence
565 boundaries caused by glacioeustatic sea-level lowerings are linked with global $\delta^{18}O$ increases (Browning
566 et al., 1996; Miller et al., 1998; Miller and Mountain, 1996). All the eight $\delta^{18}O$ events which occurred
567 during the Oligocene correspond to sea-level lowstand of 3rd order sequences (Miller et al., 1998; Pekar
568 and Miller, 1996; Pekar et al., 2002, 2000). Moreover, Boulila *et al.* (2011) compared long-period
569 obliquity modulations and global $\delta^{18}O$ increases since the Early Oligocene. These authors showed that
570 the average duration of glacioeustatic sequences during the Oligocene is 1.14 Ma, most of them
571 coinciding with one obliquity minima (node) of the ~ 1.2 Ma modulation cycles (Fig. 14). They also
572 interpreted that obliquity forcing is the major control on glacioeustatic change and creation of 3rd order
573 sequence boundaries for the time laps between 42 and 8 Ma.

574 The integration in Fig. 14 between the depositional age of the SB Mbr. and the results by Boulila
575 *et al.* (2011) shows that the GAUES formation would fit with a 3rd order glacioeustatic sequence
576 boundary caused by obliquity. The corresponding $\delta^{18}O$ event is "*Oi1a*" and induced a hiatus whose base
577 is aged at 32.9 Ma (Fig. 14), in response to an apparent sea-level fall of 43 m (Pekar et al., 2005).

578

579 ***5.1.3. Combination of tectonics and climate***

580 As previously discussed, the GAUES should result from the combination between the initiation of
581 a regional slope toward the NW and an eustatic sea-level lowering. However, the E-W orientation of the
582 La Bonette Canyon appears to be an anomaly, as the orientation is offset by 30-40° to the south in
583 relation to the direction of the regional slope which existed during deposition of the Annot Sandstones.
584 (Figs 1A, 3B).

585 Within the Southern French Alpine Foreland Basin, the Colombart Structure is anomalous because
586 it constitutes the only Oligocene fault family of E-W orientation and of pluri-kilometric extension
587 (Labaume et al., 1989). The same observation can be made concerning the La Bonette Canyon, since the
588 GAUES shows no equivalent erosive structure in other sub-basins. As the deepest points of the GAUES
589 are constrained within the Colombart Structure, the E-W orientation of the La Bonette Canyon is clearly
590 controlled by the Colombart Structure itself rather than by the regional slope. We suggest that the
591 Colombart Structure activity has favoured the GAUES excavation by channelizing submarine currents
592 in a specific narrow area of the basin, and then controlled the orientation of the La Bonette Canyon (Figs
593 3A, 3B), its cross-section asymmetry (Fig. 5), and small-scale morphology, but did not trigger its first
594 stage of formation.

595 As the GAUES does not exist within older sub-basins (i.e. Vintimiglia and Peira Cava sub-basins),
596 the submarine erosion could have resulted from the combination of three main factors, which are:

597 - a tilting with a north-westward component of the northern sub-basins occurring during the Early
598 Rupelian. It allowed the initiation of a regional slope, essential for a submarine erosion to take
599 place via the action of gravity processes. The newly formed slope angle is still very difficult to
600 quantify. In the study area, the present-day dip of the Annot Sandstones is of 10-15° on average
601 but this resulted from tectonic phase(s) occurring after the excavation of the La Bonette Canyon.
602 The dip angle can also locally change depending on the underlying structural dipping of the
603 canyon substratum (Fig. 5). As a consequence, we can only make the assumption that the intial
604 tilting was low, of just a few degrees, so probably not large alone to generate large-scale and/or
605 high-energy gravity processes explaining the intensity of the erosion that affected the Annot
606 Sandstones,
607 - a 3rd order sea-level fall (the *Oi1a* $\delta^{18}O$ event, Fig. 14) which certainly favoured the
608 destabilization of the Annot Sandstones located at shallower depths, as it is described for outer
609 shelf/upper continental slope environments during Pleistocene and Holocene low sea levels
610 (Maslin et al., 2005; Nelson et al., 2011; Rothwell et al., 1998; Wang et al., 2014).

- The appearance and subsequent increase in frequency and volume over time of gravity flows resulting from the advance of the Autapie nappe from the east or north-east (Kerckhove, 1975, 1969), with increasing erosive power on the Annot Sandstones. The triggering of submarine landslides reworking exotic materials transported over long distances, can indeed produce locally strong erosion of the bedrock, particularly in areas of abrupt change in the slope gradient (Joanne et al., 2013; Ogata et al., 2019). The latter promotes the inertial stress transfer from the slide mass to the substrate, particularly when well-lithified blocks are involved, that may cut into subsurface for tens to hundreds of meters (Joanne et al., 2013; Ogata et al., 2019). This hypothesis implies that the nappe could have formed a submarine relief (Kerckhove, 1975, 1969) or even emerged, that would have promoted and controlled the location and timing of the erosional features, i.e. as early as biozone NP22.

5.1.4. Retrogressive erosion as a dominant excavation process of the La Bonette Canyon

Two main processes may act synchronously or separately to excavate a canyon axis (Jobe et al., 2011; Pratson et al., 1994; Pratson and Coakley, 1996; Shepard, 1981; Wu et al., 2022): (i) upslope retrogressive failures leading to the formation of a blind or slope-confined canyon (Harris and Whiteway, 2011; McAdoo et al., 1997; Orange and Breen, 1992), eventually leading to a canyon head that cuts into the shelf break (Farre et al., 1983), or (ii) direct sediment supply coming from onland drainage basins and leading to a downslope incision by gravity flows. The latter can also result from the capture of particles by the canyon head, delivered by hyperpycnal currents generated during river floods (Mulder et al., 2003), or by cascading currents (Canals et al., 2009), or transported by longshore or shelf drift currents (Canals et al., 2006; Covault et al., 2007; Lewis and Barnes, 1999; Mazières et al., 2014).

The GAUES constitutes an erosion surface separating the Marnes Brunes Supérieures Member (upper Annot Sandstones, Fig. 1B) in the Trois Evêchés Sub-basin (Etienne et al., 2013; Inglis et al., 1981; Ravenne et al., 1987) and the Schistes Bruns Member (lower Schistes à Blocs Formation., Fig. 1B). Consequently, the deposition of those members is the result of an increasing sediment starvation of the northern part of the basin. This process is controlled by the southwestward migration of regional subsidence, causing the upstream accumulation of coarse-grained sediments within the Saint-Antonin fan-delta (Euzen et al., 2004).

Consequently, the stratigraphic location of the GAUES within this retrogradation trend is problematic and implies the La Bonette Canyon was probably not connected to rivers. It could be thus considered as a slope-confined canyon (Harris and Whiteway, 2011; McAdoo et al., 1997; Orange and Breen, 1992). Following this hypothesis, the main sedimentary process acting for the LBC excavation was not a downslope erosion by gravity flows generated by direct supply from land, but retrogressive

erosion through landsliding processes. It is particularly common in a convergent setting to reach a new slope equilibrium, where tectonics causes increasing slope angles and so commonly generates mass wasting events (Deffontaines et al., 2016; Festa et al., 2016; Hill et al., 2020; Kawamura et al., 2012; Lehu et al., 2015; Moore et al., 2015), including landsliding of previously deposited deep-marine series (Moore et al., 2019; Mutti et al., 2003; Park et al., 2019). Evidence for retrogressive erosion and failures as a dominant process can also be deduced from the GAUES morphology, but this point will be discussed below.

5.2. Processes shaping the La Bonette Canyon

The GAUES exhibits a sharp step-like morphology consisting of centimetric to pluri-decametric high walls with slopes ranging from 60° to sub-vertical (Fig. 8), erosive ramps with more gentle dipping slopes of about 10-20°, and flats sup-parallel to the Annot Sandstones bedding (Fig. 8). In marine environments, the formation and the preservation of steep canyon walls raise the question of the state of consolidation of the material. We discuss in the following sections the different processes shaping the GAUES from the bed scale to the submarine canyon network, which takes into account the association of diagenesis, retrogressive erosion and structural control by normal faults.

5.2.1. Influence of early lithification of the Grès d'Annot Formation

On modern margins, submarine canyons commonly exhibit flanks with slope angles > 10° (Pratson et al., 2007). Flanks are considered steep when their slope value is > 30° (Bernhardt et al., 2015; Robert et al., 2015; Trotter et al., 2019). Nevertheless, sub-vertical walls as we observed within the LBC appears to be rare, and limited to canyons cutting through well stratified carbonates, as revealed by submersible or ROV dives on the margins of New England (Ryan et al., 1978), Bahamas Sea (Mullins et al., 1982), Florida (Paull et al., 1990a, 1990b), New Jersey (Chaytor et al., 2016; McHugh et al., 1993), Celtic Sea (Carter et al., 2018; Huvenne et al., 2011), Bay of Biscay (Gillet et al., 2019), and Western Australia (Trotter et al., 2019). The best described example of the role played by the bedrock lithication in canyon excavation is the Hendrickson Canyon of the New Jersey margin, where a differential diagenesis is observed within the bedrock composed of interbedded chalks and porcelanite. The latter constitutes indurated levels resulting from *in situ* opal transition, which generates a second dewatering phase following compaction (McHugh et al., 1993). Both lithologies are cut by sub-vertical rockwalls, but porcellanite also forms broad and flat canyon floors and terraces (McHugh et al., 1993), giving a step-like morphology similar to the one of the La Bonette Canyon (Figs 4, 5, 6, and 8).

In the case of the Hendrickson Canyon, this binary morphology results from two linked processes of the secondary dewatering: (1) chalk cementation causing reduction of porosity and an increase of pore

pressure, and (2) a dense network of fracturing joints cutting through limestones at all scales, which is developed using vertical dewatering paths and subhorizontal bedding planes (McHugh et al., 1993). The combination of these processes finally leads to the excavation by slabbing or spalling following indurated levels and vertical hexagonal joints, and the formation of rectangular blocks and talus slopes (McHugh et al., 1993). Moreover, expansion of tension-release fractures leads to more exfoliation, allowing the retrogressive erosion process to be self-sustaining (McHugh et al., 1993). The same type of excavation linked to jointing is identified within mudstones and chalks composing the bedrock of the Whittard (Carter et al., 2018) and Perth (Trotter et al., 2019) canyons.

Although bedrocks of the La Bonette Canyon and the Hendrickson Canyon are different, we interpret that the Annot Sandstones reacted similarly as chalks and porcellanite to submarine erosion. From previous studies done in the Sanguinière-Restefond Sub-basin (Labaume et al., 2008; Stanley, 1961), an early diagenesis of the Grès d'Annot Formation likely occurred before the incision of the GAUES since an early calcite cement is observed in the coarse-grained sandstone beds in contact with shaly levels. Stanley (1961) suggested that the high sedimentation rate of turbidites induced a rapid burial of the sandstone deposits and would have caused hydroplastic deformation of shaly levels. The latter would have generated a pressure-solution phenomenon of the carbonate fraction of shales which precipitated under low temperatures as an early calcite phase within porous and permeable coarse-grained beds (Labaume et al., 2008; Stanley, 1961). Calcite cementation reduced the porosity and the permeability of coarse-grained beds and favoured their induration, thus creating rheological heterogeneities within the LBC substratum. The initiation of, and then the increase of the slope angle of the basin after the deposition of the Annot Sandstones would have been high enough to initiate mass-wasting processes, using the strati-mechanics resulting from the differential and stratiform cementation of turbidites. From this stage, the GAUES developed and propagated via retrogressive erosion (Pratson and Coakley, 1996).

The pressure-solution phenomenon of the carbonate fraction of shales would have also been favoured by the mixing of marine and continental waters (Labaume et al., 2008). The circulation of fresh waters from land and coastal aquifers is more and more observed on modern continental shelves and it is known to promote the recurrent triggering of failures on both passive (Kelner et al., 2016) and active margins (Orange and Breen, 1992) by generating excess pore pressures, damaging the cohesion of the deposits and lowering their internal threshold angle (Iverson and Major, 1986; Kelner et al., 2016). Fresh water flow is also thought to participate in canyon formation along passive margins (Paull et al., 1990b). Thus, this process could have also played a role in destabilizing the Annot Sandstones to initiate the GAUES.

5.2.2. Normal faults vs sedimentary processes controlling the formation of canyon steep walls

Our study of the GAUES shows that all the faults are associated with steep walls or erosive ramps (Figs 4, 6, 7, 8), but that the contrary is not true (Figs 8C, 8E, 8F). The question therefore arises about the role played by both the normal faults and the sedimentary processes in the formation of the walls shaping the LBC flanks.

The narrow F1-F2 hemi-graben is segmented in many 100 m-wide grabens and half-grabens. These structures consequently guide a high-frequency spatial succession of wall/ramp-and-terrace pairs (Figs. 5-6). But which hectometric-high rockwall are controlled/guided by a syn-sedimentary faults, and which proportion of them are major faults? We identified nine submarine scarps exhibiting a height equal or greater than 60 m, and which are located directly above or near to a fault plane (Tab. 2). Among them, seven are controlled by a major fault, i.e. exhibiting a vertical offset of 80 m or more during the canyon incision (Tab. 2). Five submarine scarps which are 90 m-high or greater are controlled by one major fault (Tab. 2). Thus, in the case of the GAUES, the higher rockwalls are controlled by major normal faults (Tab. 2), which were active during the deposition of the Grès d'Annot Formation and/or the Schistes à Blocs Formation, whereas minor faults mainly guided the creation of smaller scale erosive features. Although this relationship exits, most of the walls are higher than the vertical displacement that occurred along the fault planes, suggesting an important role also played by sedimentary processes in their formation. The steep walls are also sharp and linear in shape, which could correspond to failure planes affecting the lithified Annot Sandstones. This interpretation is more particularly evidenced where slumped/deformed beds and blocks of Annot Sandstones are found at the base or against the walls (Figs 7B, 8C, 12). Following this interpretation, the normal faults would have guided and controlled the location and the vertical propagation of failure planes. The triggering of the failures could then have multiple causes: the activity of the faults themselves or the retrogressive erosion within the central and deepest part of the La Bonette Canyon which modified the slope equilibrium and forced the unstable lateral areas of the flanks of the canyon to glide downstreamward. Consequently, within partially lithified sandstone turbidites, sealed or active major faults would control the formation and location of the highest and steepest walls (or erosive ramps), and retrogressive landsliding processes used major faults to propagate, i.e as it does through unconsolidated sediments (Mercier et al., 2023). The question of what is the maximum possible rockwall height which can be created within lithified turbidites is still open, since the creation of the La Bonette Canyon occurred in a relatively active tectonic setting, that limited the stability of the higher rockwalls. The infilling of the La Bonette Canyon by the Schistes à Blocs Formation also probably limited the time of formation and evolution of the submarine scarps.

In the absence of normal faults, walls also formed but they are smaller and gentler. The superposition of several wall-terrace pairs along a single flank of the La Bonette Canyon suggest

multiple phases for their formation, as it is observed along modern canyons (Babonneau et al., 2002; Baztan et al., 2005; Deptuck et al., 2007; Paull et al., 2013; Wu et al., 2022). In this case, the formation and propagation of the axial incision of the La Bonette Canyon would have locally increased the slope angle at the base of the lateral flanks. This would have then promoted the triggering of several small-scale retrogressive failures, the base of each failure plane rooting along a shalier interval and creating a terrace (Fig. 8E). Few slumped Annot Sandstone beds and blocks were found associated with these superimposed low-elevation wall-terrace pairs, suggesting the low volumes of remobilized material were rapidly evacuated downstreamward.

5.2.3. Control of the asymmetrical cross-section profile by the Colombart Structure

As described in section 4.2, the La Bonette Canyon exhibits a V-shaped and asymmetrical cross-section profile, composed of a southern gentler flank, a thalweg and the northern steeper flank. The asymmetry of the cross-section profile is expressed in two different ways between the two canyon flanks: (i) a difference in width and slope angle (Tab. 1), and (ii) a difference in depth/height of each interfuve (Figs 3B, 5).

The smaller width and the greater slope angle of the northern canyon flank correlate with the narrow F1-F2 hemi-graben and the high spatial density of steep rockwalls separated by narrow terraces. On the opposite, the longer and gentler southern flank correlates with the larger F3-F6 hemi-graben, the presence of erosive ramps and larger terraces. This difference of morphology between the two canyon flanks corresponds to a direct control by the Colombart Structure, which is itself asymmetrical, as detailed in section 4.1.

This is consistent with the cross-section profiles observed for present or ancient canyon systems, which are axially controlled by a tectonic structure whose activity is syn-sedimentary, such as a fold-and-thrust like structure (Micallef et al., 2014; Mountjoy et al., 2009) or a growth fault and rollover fold (Mercier et al., 2023). Therefore, whatever the structural context, it is the asymmetry of the syn-sedimentary deformation that is directly responsible for the asymmetry of the transverse profile of the canyon (Mercier et al., 2023).

However, the structural control does not explain the difference of depth estimated between the southern and northern interfluves of the transverse profile of the La Bonette Canyon (Fig. 5). This difference should come from a stronger erosion that affected the northern interfluve as the elevation of the GAUES above the Debrite Key Level 1 is lower here than on the southern interfluve (Fig. 5). A similar significant difference in erosion intensity between the two canyon flanks was also evidenced in the Afam Canyon system (Mercier et al., 2023) and along the Kaoping Canyon (Chiang and Yu, 2006; Liu et al., 1993), where conduits are sub-perpendicular to the orientation of the local slope gradient

781 because of their control by tectonic structures. It can therefore be concluded that the northward
782 deepening of the cross-section profile of the La Bonette Canyon suggests that the basin slope exhibited
783 a northward (local?) dipping component during the canyon formation, and that the La Bonette Canyon
784 was therefore oriented sub-perpendicular to this slope, because of its control by the Colombart Structure.
785 This is coherent with a slope direction that can be deduced from northwestward to northward
786 paleocurrent directions measured within the Annot Sandstones by Jean *et al*. (1985) before the initiation
787 of the GAUES.
788
789 ***5.2.4. Rectangular drainage pattern***
790 The La Bonette and the L'Alpe tributaries are sub-perpendicular to the axis of the La Bonette
791 Canyon (Figs 3A, 3B). The L'Alpe tributary intersected the La Bonette Canyon within the F1-F2 hemi-
792 graben, as it is also assumed for the La Bonette tributary due to its orientation (Fig. 3A). In its preserved
793 part, the Baisse de la Plate tributary is axially controlled by F6, but its deepening towards the east
794 required a change of orientation of its course close to 90° in order to be captured by the La Bonette
795 Canyon, which deepens westward (Figs 3A, 3B). In the Afam Canyon system which is also controlled
796 by normal faults and rollovers, tributaries whose the upstream part is opposite to the orientation of the
797 main canyon are observed (Mercier et al., 2023). This feature is due to their development by
798 retrogressive erosion cutting through a roll-over forelimb which exhibits local counter-slopes. Thus, the
799 direction of deepening of the preserved part of the Baisse de la Plate tributary might result from its
800 control by the rollover of the Colombart Structure.
801 Therefore, because of its specific features including (i) an axial control of the LBC thalweg and
802 the Baisse de la Plate tributary by faults oriented perpendicular to the local slope, (ii) a 90° change in
803 the orientation of the Baisse de la Plate tributary, (iii) the capture by the LBC thalweg of the L'Alpe,
804 Baisse de la Plate and La Bonette tributaries at an angle close to 90° (Figs 3A, 3B, 15), the La Bonette
805 Canyon can be interpreted as a submarine rectangular drainage network (Mercier et al., 2023; Zernitz,
806 1932). The orientation of the preserved part of the Restefond tributary shows it was probably captured
807 by the downstream course of the outcropping La Bonette Canyon, but at an angle close to 45°. Following
808 this interpretation, only two main order tributaries could be identified for the La Bonette Canyon, a 2nd
809 order corresponding to the thalweg of the La Bonette Canyon and a 1st order to the secondary tributaries,
810 while up to 6 orders are identified within the Afam Canyon system (Mercier et al., 2023). Consequently,
811 we can only assume that many orders corresponding to smaller tributaries should have also shaped the
812 La Bonette Canyon but they have not been preserved within the stratigraphic record due to phases of
813 erosion that affected the area.

Finally, the elongated depressions located on both sides of the Caserne de Restefond (Figs 3A, 3B) cannot be clearly connected to the LBC drainage network and may therefore correspond to gullies cutting through the northern part of the Sanguinière-Restefond Sub-basin. Their westward orientation, parallel to the La Bonette Canyon, demonstrates anyway the westward component of the local slope. In addition to the northward downsloping interpreted from the transverse profile of the La Bonette Canyon (Fig. 5), this suggests that the main downslope direction of the Sanguinière-Restefond Sub-basin was oriented westward or northwestward during NP22-lower NP23 (Fig. 15).

6. Conclusions

Through combined sedimentological, structural and paleontological analyses of the outcrops we reconstructed the Rupelian history of a submarine canyon, the La Bonette Canyon, excavated 700 m deep within the Grès d'Annot Formation in the internal part of the Southern French Alpine Foreland Basin. The planform pattern of the basal erosive surface of the canyon, named the Grès d'Annot Upper Erosion Surface, was reconstructed using a GIS modelling. The structural reconstruction allowed geometrical comparisons with subsurface examples coming from the literature, then provided an integrated picture of the canyon development in which multi-scale morphology of the canyon was largely driven by the action of extensive structures and gravity processes. We also provide for the first time a chronological constraint on canyon incision by dating the Schistes à Blocs Formation which was deposited immediately on top of the erosional surface during biozones NP22-lower NP23 in the Sanguinière-Restefond Sub-basin.

The N80°E orientation of the canyon as well as the multi-scale morphology of its transverse profile result from the axial control by the Colombart Structure, which is composed of two main faults with southward vergence and hectometric vertical offset, as well as a northward dipping roll-over. Extensional structures were active during canyon excavation. At the sub-basin scale, they controlled the capture of tributaries at right angles in respect to orientation of the La Bonette Canyon, which draws a rectangular drainage pattern. They generated an asymmetrical cross-section profile of the canyon, but also controlled the thalweg morphology and its axial incision position. At a smaller scale, they commonly influence the location of many erosive walls, terraces and ramps, but those elementary features of the GAUES are not necessarily controlled by faults. They can reach one hundred meters of height and mainly result from retrogressive erosion affecting the partially lithified Annot Sandstones. Finally, the deformation of the rollover forelimb during the canyon infilling by the Schistes à Blocs Formation favoured the triggering of submarine landslides oriented along or toward the thalweg.

The submarine erosion resulted from the addition of three main factors, namely: i) a possible tilting of the basin towards the west or north-west, which triggered numerous retrogressive submarine landslides

and gravity processes, ii) the 3rd order eustatic fall linked to the *Oi1a* $\delta^{18}O$ event, and iii) the increasing erosive power of gravity currents which were sourced from the remobilized front of the Autapie nappe during its advance in the basin.

Data avaibility

Data will be made available on reasonable request.

Acknowledgments

Louison Mercier was a PhD student funded by TotalEnergies and the ANRT, and the redaction of this paper has been done thanks to the financial support of UMR7329 Géoazur. Sampling and photography using a drone were carried out with the authorisation of the director of the Parc National du Mercantour. The authors acknowledge the journal editor Roberto Tinterri, an anonymous reviewer and Julian Clark for the comments and suggestions that greatly clarified the paper.

References

Allin, J.R., Hunt, J.E., Clare, M.A., Talling, P.J., 2017. Eustatic sea-level controls on the flushing of a shelf-incising submarine canyon. GSA Bulletin 130, 222–237. https://doi.org/10.1130/B31658.1

Almeida, N.M. de, Vital, H., Gomes, M.P., 2015. Morphology of submarine canyons along the continental margin of the Potiguar Basin, NE Brazil. Marine and Petroleum Geology 68, 307–324. https://doi.org/10.1016/j.marpetgeo.2015.08.035

Alves, T.M., Lourenço, S.D.N., 2010. Geomorphologic features related to gravitational collapse: Submarine landsliding to lateral spreading on a Late Miocene–Quaternary slope (SE Crete, eastern Mediterranean). Geomorphology 123, 13–33. https://doi.org/10.1016/j.geomorph.2010.04.030

Anderson, K.S., Graham, S.A., Hubbard, S.M., 2006. Facies, Architecture, and Origin of a Reservoir-Scale Sand-Rich Succession Within Submarine Canyon Fill: Insights from Wagon Caves Rock (Paleocene), Santa Lucia Range, California, U.S.A. Journal of Sedimentary Research 76, 819–838. https://doi.org/10.2110/jsr.2006.066

Apps, G., 1985. The Grès d'Annot foreland basin, Haute Provence: the control of turbidite deposition by structurally induced basin floor topography. Presented at the 6th European Regional Meeting of Sedimentology IAS Lleida, pp. 18–21.

Apps, G., Peel, F., Elliott, T., 2004. The structural setting and paleogeographical evolution of the Grès d'Annot Basin, in: P. Joseph & A. Lomas, Eds., Deep-Water Sedimentation in the Alpine Foreland Basin of SE France: New Perspectives on the Grès d'Annot and Related Systems, Geological Society Special Publications. London, pp. 65–96.

ArcGIS Pro 3.1 Topo to Raster tool, n.d.

Babonneau, N., Savoye, B., Cremer, M., Klein, B., 2002. Morphology and architecture of the present canyon and channel system of the Zaire deep-sea fan. Marine and Petroleum Geology 19, 445–467. https://doi.org/10.1016/S0264-8172(02)00009-0

Baztan, J., Berné, S., Olivet, J.-L., Rabineau, M., Aslanian, D., Gaudin, M., Réhault, J.-P., Canals, M., 2005. Axial incision: The key to understand submarine canyon evolution (in the western Gulf of Lion). Marine and Petroleum Geology, The Gulf of Lions: an overview of recent studies within the French "Margins" Programme 22, 805–826. https://doi.org/10.1016/j.marpetgeo.2005.03.011

Bernhardt, A., Melnick, D., Jara-Muñoz, J., Argandoña, B., González, J., Strecker, M.R., 2015. Controls on submarine canyon activity during sea-level highstands: The Biobío canyon system offshore Chile. Geosphere 11, 1226–1255. https://doi.org/10.1130/GES01063.1

Bolli, H.M., Beckmann, J.P., Saunders, J. B., Saunders, John B., 1994. Benthic Foraminiferal Biostratigraphy of the South Caribbean Region. Cambridge University Press, Cambridge, https://doi.org/10.1017/CBO9780511564406.

Boulila, S., Galbrun, B., Miller, K.G., Pekar, S.F., Browning, J.V., Laskar, J., Wright, J.D., 2011. On the origin of Cenozoic and Mesozoic "third-order" eustatic sequences. Earth-Science Reviews 109, 94–112. https://doi.org/10.1016/j.earscirev.2011.09.003

Bourget, J., Zaragosi, S., Ellouz-Zimmermann, N., Mouchot, N., Garlan, T., Schneider, J.-L., Lanfumey, V., Lallemant, S., 2011. Turbidite system architecture and sedimentary processes along topographically complex slopes: the Makran convergent margin. Sedimentology 58, 376–406. https://doi.org/10.1111/j.1365-3091.2010.01168.x

Bouroullec, R., Cartwright, J.A., Johnson, H.D., Lansigu, C., Quémener, J.-M., Savanier, D., 2004. Syndepositional faulting in the Grès d'Annot Formation, SE France: high-resolution kinematic analysis and stratigraphic response to growth faulting. Geological Society, London, Special Publications 221, 241–265. https://doi.org/10.1144/GSL.SP.2004.221.01.13

Browning, J.V., Miller, K.G., Pak, D.K., 1996. Global implications of lower to middle Eocene sequence boundaries on the New Jersey coastal plain: The icehouse cometh. Geology 24, 639–642. https://doi.org/10.1130/0091-7613(1996)024<0639:GIOLTM>2.3.CO;2

Campredon, R., 1972. Les formations paléogènes des Alpes maritimes franco-italiennes, Thèse de l'Université de Nice.

Canals, M., Danovaro, R., Heussner, S., Lykousis, V., Puig, P., Trincardi, F., Calafat, A.M., De Madron, X.D., Palanques, A., Sànchez-Vidal, A., 2009. Cascades in Mediterranean Submarine Grand Canyons. Oceanography 22, 26–43.

Canals, M., Puig, P., de Madron, X.D., Heussner, S., Palanques, A., Fabres, J., 2006. Flushing submarine canyons. Nature 444, 354–357. https://doi.org/10.1038/nature05271

Carter, G.D.O., Huvenne, V.A.I., Gales, J.A., Lo Iacono, C., Marsh, L., Ougier-Simonin, A., Robert, K., Wynn, R.B., 2018. Ongoing evolution of submarine canyon rockwalls; examples from the Whittard Canyon, Celtic Margin (NE Atlantic). Progress in Oceanography, Bridging the gap between the shallow and deep oceans: The key role of submarine canyons 169, 79–88. https://doi.org/10.1016/j.pocean.2018.02.001

Cavailhes, T., Labaume, P., Sizun, J.-P., Soliva, R., Gout, C., Potdevin, J.-L., Buatier, M., Gay, A., Chauvet, A., Charpentier, D., Travé, A., 2014. Difference in petrophysical properties between foliated and dilatant fault rocks in deeply buried clastics: The case of the Grès d'Annot Formation, SW French Alps. Terra Nova 26, 298–306. https://doi.org/10.1111/ter.12100

Cavailhes, T., Soliva, R., Labaume, P., Wibberley, C., Sizun, J.-P., Gout, C., Charpentier, D., Chauvet, A., Scalabrino, B., Buatier, M., 2013. Phyllosilicates formation in faults rocks: Implications for dormant fault-sealing potential and fault strength in the upper crust. Geophysical Research Letters 40, 4272–4278. https://doi.org/10.1002/grl.50829

Chaytor, J.D., Demopoulos, A.W.J., ten Brink, U.S., Baxter, C., Quattrini, A.M., Brothers, D.S., 2016. Assessment of Canyon Wall Failure Process from Multibeam Bathymetry and Remotely Operated Vehicle (ROV) Observations, U.S. Atlantic Continental Margin, in: Lamarche, G., Mountjoy, J., Bull, S., Hubble, T., Krastel, S., Lane, E., Micallef, A., Moscardelli, L., Mueller, C., Pecher, I., Woelz, S. (Eds.), Submarine Mass Movements and Their Consequences: 7th International Symposium, Advances in Natural and Technological Hazards Research. Springer International Publishing, Cham, pp. 103–113. https://doi.org/10.1007/978-3-319-20979-1_10

Chiang, C.-S., Yu, H.-S., 2006. Morphotectonics and incision of the Kaoping submarine canyon, SW Taiwan orogenic wedge. Geomorphology 80, 199–213. https://doi.org/10.1016/j.geomorph.2006.02.008

941 Cicha, L., Rögl, F., Rupp, C., Ctyroka, J., 1998. Oligocene-Miocene foraminifera of the Central
942 Paratethys, Verlag Waldemar Kramer. ed. Frankfurkt am Main.
943 Clayton, C.A., Olariu, C., 2022. Tectonic preconditioning of recurrent large scale canyon incisions;
944 example from Cretaceous and Paleogene of northern Gulf of Mexico. Marine Geology 453,
945 106909. https://doi.org/10.1016/j.margeo.2022.106909
946 Collot, J.-Y., Ratzov, G., Silva, P., Proust, J.-N., Migeon, S., Hernandez, M.-J., Michaud, F., Pazmino,
947 A., Castillo, D.B., Alvarado, A., Khurama, S., 2019. The Esmeraldas Canyon: A Helpful Marker
948 of the Pliocene-Pleistocene Tectonic Deformation of the North Ecuador-Southwest Colombia
949 Convergent Margin. Tectonics 38, 3140–3166. https://doi.org/10.1029/2019TC005501
950 Covault, J.A., Normark, W.R., Romans, B.W., Graham, S.A., 2007. Highstand fans in the California
951 borderland: The overlooked deep-water depositional systems. Geology 35, 783–786.
952 https://doi.org/10.1130/G23800A.1
953 Deffontaines, B., Liu, C.-S., Hsu, H.-H., 2016. Structure and deformation of the Southern Taiwan
954 accretionary prism: The active submarine Fangliao Fault Zone offshore west Hengchun
955 Peninsula. Tectonophysics, Geodynamics and Environment in East Asia, GEEA 2014 692, 227–
956 240. https://doi.org/10.1016/j.tecto.2016.11.007
957 Deptuck, M.E., Sylvester, Z., Pirmez, C., O'Byrne, C., 2007. Migration–aggradation history and 3-D
958 seismic geomorphology of submarine channels in the Pleistocene Benin-major Canyon, western
959 Niger Delta slope. Marine and Petroleum Geology, Sinuous Deep-Water Channels: Genesis,
960 Geometry and Architecture 24, 406–433. https://doi.org/10.1016/j.marpetgeo.2007.01.005
961 Di Celma, C., 2011. Sedimentology, architecture, and depositional evolution of a coarse-grained
962 submarine canyon fill from the Gelasian (early Pleistocene) of the Peri-Adriatic basin, Offida,
963 central Italy. Sedimentary Geology 238, 233–253. https://doi.org/10.1016/j.sedgeo.2011.05.003
964 Di Celma, C., Cantalamessa, G., Didaskalou, P., 2013. Stratigraphic organization and predictability of
965 mixed coarse-grained and fine-grained successions in an upper slope Pleistocene turbidite system
966 of the Peri-Adriatic basin. Sedimentology 60, 763–799. https://doi.org/10.1111/j.1365-
967 3091.2012.01359.x
968 Di Celma, C., Teloni, R., Rustichelli, A., 2016. Evolution of the Gelasian (Pleistocene) slope turbidite
969 systems of southern Marche (Peri-Adriatic basin, central Italy). Journal of Maps 12, 137–151.
970 https://doi.org/10.1080/17445647.2014.995724
971 Di Celma, C., Teloni, R., Rustichelli, A., 2014. Large-scale stratigraphic architecture and sequence
972 analysis of an early Pleistocene submarine canyon fill, Monte Ascensione succession (Peri-
973 Adriatic basin, eastern central Italy). Int J Earth Sci (Geol Rundsch) 103, 843–875.
974 https://doi.org/10.1007/s00531-013-0984-3
975 du Fornel, E., 2003. Reconstitution sédimentologique tridimensionnelle et simulation stratigraphique du
976 système turbiditique éocène des grès d'Annot (Alpes méridionales). Université de Rennes 1.
977 du Fornel, E., Joseph, P., Desaubliaux, G., Eschard, R., Guillocheau, F., Muller, C., Ravenne, C.,
978 Sztràkos, K., 2004. The southern Grès d'Annot Outcrops (French Alps): an attempt at regional
979 correlation, in: P. Joseph & A. Lomas, Eds., Deep-Water Sedimentation in the Alpine Foreland
980 Basin of SE France: New Perspectives on the Grès d'Annot and Related Systems, Geological
981 Society Special Publications. London, pp. 137–160.
982 Dumont, T., Simon-Labric, T., Authemayou, C., Heymes, T., 2011. Lateral termination of the north-
983 directed Alpine orogeny and onset of westward escape in the Western Alpine arc: Structural and
984 sedimentary evidence from the external zone. Tectonics 30.
985 https://doi.org/10.1029/2010TC002836
986 Elliott, T., Apps, G., Davies, H., Evans, M., Ghibaudo, G., Graham, R.H., 1985. Field excursion B: a
987 structural and sedimentological traverse through the tertiary foreland basin of the external Alps
988 of South-East France, in: International Symposium on Foreland Basins - Excursion Guidebook.
989 Frigboug, Switzerland, pp. 39–73.

990 Etienne, S., Mulder, T., Razin, P., Bez, M., Désaubliaux, G., Joussiaume, R., Tournadour, E., 2013.
991 Proximal to distal turbiditic sheet-sand heterogeneities: Characteristics of associated internal
992 channels. Examples from the Trois Evêchés area, Eocene-Oligocene Annot Sandstones (Grès
993 d'Annot), SE France. Marine and Petroleum Geology, Special Issue: Internal architecture,
994 bedforms and geometry of turbidite channels 41, 117–133.
995 https://doi.org/10.1016/j.marpetgeo.2012.03.007
996 Euzen, T., Joseph, P., Fornel, E.D., Lesur, S., Granjeon, D., Guillocheau, F., 2004. Three-dimensional
997 stratigraphic modelling of the Grès d'Annot system, Eocene-Oligocene, SE France. Geological
998 Society, London, Special Publications 221, 161–180.
999 https://doi.org/10.1144/GSL.SP.2004.221.01.09
1000 Farre, J.A., McGregor, B.A., Ryan, W.B.F., Robb, J.M., 1983. Breaching the shelf break: Passage from
1001 youthful to mature phase in submarine canyon evolution, in: Society of Economic
1002 Paleontologists and Mineralogists Special Publication. Tulsa, Oklahoma, pp. 25–39.
1003 Festa, A., Ogata, K., Pini, G.A., Dilek, Y., Alonso, J.L., 2016. Origin and significance of olistostromes
1004 in the evolution of orogenic belts: A global synthesis. Gondwana Research 39, 180–203.
1005 https://doi.org/10.1016/j.gr.2016.08.002
1006 Ford, M., Duchêne, S., Gasquet, D., Vanderhaeghe, O., 2006. Two-phase orogenic convergence in the
1007 external and internal SW Alps. Journal of the Geological Society 163, 815–826.
1008 https://doi.org/10.1144/0016-76492005-034
1009 Ford, M., Lickorish, W.H., 2004. Foreland basin evolution around the western Alpine Arc, in: P. Joseph
1010 & A. Lomas, Eds., Deep-Water Sedimentation in the Alpine Foreland Basin of SE France: New
1011 Perspectives on the Grès d'Annot and Related Systems, Geological Society Special Publications.
1012 London, pp. 39–63.
1013 Frey Martinez, J., Cartwright, J., Hall, B., 2005. 3D seismic interpretation of slump complexes: examples
1014 from the continental margin of Israel. Basin Research 17, 83–108.
1015 https://doi.org/10.1111/j.1365-2117.2005.00255.x
1016 Fulthorpe, C.S., Austin, J.A., Mountain, G.S., 2000. Morphology and distribution of Miocene slope
1017 incisions off New Jersey: Are they diagnostic of sequence boundaries? GSA Bulletin 112, 817–
1018 828. https://doi.org/10.1130/0016-7606(2000)112<817:MADOMS>2.0.CO;2
1019 Galloway, W.E., Dingus, W.F., Paige, R.E., 1991. Seismic and Depositional Facies of Paleocene-Eocene
1020 Wilcox Group Submarine Canyon Fills, Northwest Gulf Coast, U.S.A., in: Weimer, P., Link,
1021 M.H. (Eds.), Seismic Facies and Sedimentary Processes of Submarine Fans and Turbidite
1022 Systems, Frontiers in Sedimentary Geology. Springer, New York, NY, pp. 247–271.
1023 https://doi.org/10.1007/978-1-4684-8276-8_13
1024 Gillet, H., Guiastrennec-Faugas, L., Gazzoli, L., 2019. ROV submarine exploration of the proximal part
1025 of the Capbreton canyon (Bay of Biscay). Morphological surprises and discovery of cold seep-
1026 related authigenic carbonate structures. Geophysical Research Abstracts 21, 1–1.
1027 Greene, H.G., Clarke, S.H.Jr., Kennedy, M.P., 1991. Tectonic evolution of submarine canyons along the
1028 California continental margin. SEPM Special Publication 46, 231–248.
1029 Gupta, S., 1997. Tectonic control on paleovalley incision at the distal margin of the early Tertiary Alpine
1030 foreland basin, southeastern France. Journal of Sedimentary Research 67, 1030–1043.
1031 https://doi.org/10.1306/D42686BC-2B26-11D7-8648000102C1865D
1032 Han, W.-C., Liu, C.-S., Chi, W.-C., Chen, L., Lin, C.-C., Chen, S.-C., 2017. Westward advance of the
1033 deformation front and evolution of submarine canyons offshore of southwestern Taiwan. Journal
1034 of Asian Earth Sciences, Tectonics, Volcanism and Geo-energy in East Asia 149, 6–19.
1035 https://doi.org/10.1016/j.jseaes.2017.07.001
1036 Harris, P.T., Whiteway, T., 2011. Global distribution of large submarine canyons: Geomorphic
1037 differences between active and passive continental margins. Marine Geology 285, 69–86.
1038 https://doi.org/10.1016/j.margeo.2011.05.008

Hill, J.C., Watt, J.T., Brothers, D.S., Kluesner, J.W., 2020. Submarine canyons, slope failures and mass transport processes in southern Cascadia. Geological Society, London, Special Publications 500, 453–475. https://doi.org/10.1144/SP500-2019-169

Hutchinson, M.F., Xu, T., Stein, J.A., 2011. Recent Progress in the ANUDEM Elevation Gridding Procedure, in: Geomorphometry. Redlands, California, USA, pp. 19–22.

Huvenne, V.A.I., Tyler, P.A., Masson, D.G., Fisher, E.H., Hauton, C., Hühnerbach, V., Bas, T.P.L., Wolff, G.A., 2011. A Picture on the Wall: Innovative Mapping Reveals Cold-Water Coral Refuge in Submarine Canyon. PLOS ONE 6, e28755. https://doi.org/10.1371/journal.pone.0028755

IGN, n.d. RGE ALTI®.

Inglis, A., Lepvraud, E., Mousset, E., Salim, A., Vially, R., 1981. Etude sédimentologique des Grès d'Annot (région de Colmars-les-Alpes et du Col de la Cayolle)., in: ENSPM. p. 172.

Ito, M., Ishikawa, K., Nishida, N., 2014. Distinctive erosional and depositional structures formed at a canyon mouth: A lower Pleistocene deep-water succession in the Kazusa forearc basin on the Boso Peninsula, Japan. Sedimentology 61, 2042–2062. https://doi.org/10.1111/sed.12128

Ito, M., Saito, T., 2006. Gravel Waves in an Ancient Canyon: Analogous Features and Formative Processes of Coarse-Grained Bedforms in a Submarine-Fan System, the Lower Pleistocene of the Boso Peninsula, Japan. Journal of Sedimentary Research 76, 1274–1283. https://doi.org/10.2110/jsr.2006.093

Iverson, R.M., Major, J.J., 1986. Groundwater Seepage Vectors and the Potential for Hillslope Failure and Debris Flow Mobilization. Water Resources Research 22, 1543–1548. https://doi.org/10.1029/WR022i011p01543

Jackson, C.A.-L., McAndrew, A.E., Hodgson, D.M., Dreyer, T., 2021. Repeated degradation and progradation of a submarine slope over geological timescales. Journal of Sedimentary Research 91, 116–145. https://doi.org/10.2110/jsr.2020.77

Janocko, J., Basilici, G., 2021. Architecture of coarse-grained gravity flow deposits in a structurally confined submarine canyon (late Eocene Tokaren Conglomerate, Slovakia). Sedimentary Geology 417, 105880. https://doi.org/10.1016/j.sedgeo.2021.105880

Jean, S., 1985. Les Grès d'Annot au N.W. du Massif de l'Argentera-Mercantour (zone subalpine méridionale des Alpes occidentales françaises) - Sédimentologie - Paléontologie (Thèse). Université Scientifique et Médicale de Grenoble.

Jean, S., Kerckhove, C., Perriaux, C., Ravenne, C., 1985. Un modèle paléogène de bassin à turbidites : les Grès d'Annot du NW du massif de L'Argentera-Mercantour. GA 61, 115–143.

Joanne, C., Lamarche, G., Collot, J.-Y., 2013. Dynamics of giant mass transport in deep submarine environments: the Matakaoa Debris Flow, New Zealand. Basin Research 25, 471–488. https://doi.org/10.1111/bre.12006

Jobe, Z.R., Lowe, D.R., Uchytil, S.J., 2011. Two fundamentally different types of submarine canyons along the continental margin of Equatorial Guinea. Marine and Petroleum Geology 28, 843–860.

Joseph, P., Lomas, A., 2004. Deep-water sedimentation in the Alpine Foreland Basin of SE France: New perspectives on the Grès d'Annot and related systems-an introduction, in: P. Joseph & A. Lomas, Eds., Deep-Water Sedimentation in the Alpine Foreland Basin of SE France: New Perspectives on the Grès d'Annot and Related Systems, Geological Society Special Publications. London, pp. 1–16.

Joseph, P., Ravenne, C., 2001. Overview of the Grès d'Annot basin. Presented at the Turbidite sedimentation in confined settings: Research meeting and field excursion to the Grès d'Annot, held in Nice on 10-15 september 2001, by Joseph, Lomas, Broucke, Clark, Gardiner, Guillocheau, McCaffrey, Ravenne, Robin & Stanbrook.

Kawamura, K., Sakaguchi, A., Strasser, M., Anma, R., Ikeda, H., 2012. Detailed Observation of Topography and Geologic Architecture of a Submarine Landslide Scar in a Toe of an Accretionary Prism, in: Yamada, Y., Kawamura, K., Ikehara, K., Ogawa, Y., Urgeles, R.,

Mosher, D., Chaytor, J., Strasser, M. (Eds.), Submarine Mass Movements and Their Consequences, Advances in Natural and Technological Hazards Research. Springer Netherlands, Dordrecht, pp. 301–309. https://doi.org/10.1007/978-94-007-2162-3_27

Kelner, M., Migeon, S., Tric, E., Couboulex, F., Dano, A., Lebourg, T., Taboada, A., 2016. Frequency and triggering of small-scale submarine landslides on decadal timescales: Analysis of 4D bathymetric data from the continental slope offshore Nice (France). Marine Geology 379, 281–297. https://doi.org/10.1016/j.margeo.2016.06.009

Kerckhove, C., 1975. Sédimentation chaotique & tectogénese : les olisthostromes des nappes de l'Embrunais - Ubaye (Alpes occidentales françaises), in: IXe Congrès International de Sédimentologie - Thème 4 - Tectonique et Sédimentation. Nice, pp. 195–207.

Kerckhove, C., 1969. La "zone du Flysch" dans les nappes de l'Embrunais-Ubaye (Alpes occidentales), in: Géologie Alpine. pp. 5–204.

Kerckhove, C., Monjuvent, G., 1980. Carte géologique de la France (1:250 000), feuille de Gap (35).

Kerckhove, C., Pairis, J.L., Plan, J., Schneegans, D., Gidon, M., 1974. Carte géologique de la France (1:50 000), feuille de Barcelonnette (895).

Kerckhove, C., Thouvenot, F., 2014. Carte Géologique de la France (1:50 000), feuille d'Allos (919).

Labaume, P., Jolivet, M., Souquière, F., Chauvet, A., 2008. Tectonic control on diagenesis in a foreland basin: combined petrologic and thermochronologic approaches in the Grès d'Annot basin (Late Eocene–Early Oligocene, French–Italian external Alps). Terra Nova 20, 95–101. https://doi.org/10.1111/j.1365-3121.2008.00793.x

Labaume, P., Ritz, J.-F., Philip, H., 1989. Failles normales récentes dans les Alpes sud-occidentales: leurs relations avec la tectonique compressive. C. r. Acad. sci., Sér. 2, Méc. phys. chim. sci. univers sci. terre 308, 1553–1560.

Labaume, P., Sizun, J.P., Charpentier, D., Travé, A., Chirouze, F., Buatier, M., Chauvet, A., Jolivet, M., Monié, P., Arnaud, N., 2009. Diagenesis controlled by tectonic burial in a foreland basin turbidite formation. The case example of the Grès d'Annot, French-italian external Alps, in: Geophysical Research Abstracts. Presented at the EGU General Assembly 2009, p. 3.

Lansigu, C., 2000. Mécanismes de déformation dans les failles, implications sur les circulations de fluides, in: Thèse de l'Université de Rennes 1. p. 337.

Lehu, R., Lallemand, S., Hsu, S.-K., Babonneau, N., Ratzov, G., Lin, A.T., Dezileau, L., 2015. Deep-sea sedimentation offshore eastern Taiwan: Facies and processes characterization. Marine Geology 369, 1–18. https://doi.org/10.1016/j.margeo.2015.05.013

Lewis, K.B., Barnes, P.M., 1999. Kaikoura Canyon, New Zealand: active conduit from near-shore sediment zones to trench-axis channel. Marine Geology 162, 39–69. https://doi.org/10.1016/S0025-3227(99)00075-4

Lickorish, W.H., Ford, M., 1998. Sequential restoration of the external Alpine Digne thrust system, SE France, constrained by kinematic data and synorogenic sediments. Geological Society, London, Special Publications 134, 189–211. https://doi.org/10.1144/GSL.SP.1998.134.01.09

Liu, C.-S., Lundberg, N., Reed, D.L., Huang, Y.-L., 1993. Morphological and seismic characteristics of the Kaoping Submarine Canyon. Marine Geology 111, 93–108. https://doi.org/10.1016/0025-3227(93)90190-7

Maslin, M., Vilela, C., Mikkelsen, N., Grootes, P., 2005. Causes of catastrophic sediment failures of the Amazon Fan. Quaternary Science Reviews 24, 2180–2193. https://doi.org/10.1016/j.quascirev.2005.01.016

Mauffrey, M.A., Berné, S., Jouet, G., Giresse, P., Gaudin, M., 2015. Sea-level control on the connection between shelf-edge deltas and the Bourcart canyon head (western Mediterranean) during the last glacial/interglacial cycle. Marine Geology 370, 1–19. https://doi.org/10.1016/j.margeo.2015.09.010

Mauffrey, M.-A., Urgeles, R., Berné, S., Canning, J., 2017. Development of submarine canyons after the Mid-Pleistocene Transition on the Ebro margin, NW Mediterranean: The role of fluvial

connections. Quaternary Science Reviews 158, 77–93. https://doi.org/10.1016/j.quascirev.2017.01.006

Mazières, A., Gillet, H., Castelle, B., Mulder, T., Guyot, C., Garlan, T., Mallet, C., 2014. High-resolution morphobathymetric analysis and evolution of Capbreton submarine canyon head (Southeast Bay of Biscay—French Atlantic Coast) over the last decade using descriptive and numerical modeling. Marine Geology 351, 1–12. https://doi.org/10.1016/j.margeo.2014.03.001

McAdoo, B.G., Orange, D.L., Screaton, E., Lee, H., Kayen, R., 1997. Slope basins, headless canyons, and submarine palaeoseismology of the Cascadia accretionary complex. Basin Research 9, 313–324. https://doi.org/10.1046/j.1365-2117.1997.00049.x

McHugh, C.M., Ryan, W.B.F., Schreiber, B.C., 1993. The Role of Diagenesis in Exfoliation of Submarine Canyons. AAPG Bulletin 77, 145–172. https://doi.org/10.1306/BDFF8BB4-1718-11D7-8645000102C1865D

Meckel, L.D., Ford, M., Bernouilli, D., 1996. Tectonic and sedimentary evolution of the Dévoluy Basin, a remnant of the Tertiary western Alpine foreland basin, SE France, in: Géologie de La France. pp. 3–26.

Menard, H.W., 1955. Deep-sea channels, topography and sedimentation. A.A.P.G. Bulletin 39, 236–255.

Mercier, L., Migeon, S., Dall'Asta, M., Praeg, D., Rubino, J.-L., Delhaye-Prat, V., Lafont, F., Akpi, T., 2023. Rectangular drainage pattern of a submarine canyon controlled by extensional tectonic structures: Case study of the Afam Incision Surface (Tortonian, Niger Delta, Nigeria). Marine Geology 462, 107093. https://doi.org/10.1016/j.margeo.2023.107093

Micallef, A., Mountjoy, J.J., Barnes, P.M., Canals, M., Lastras, G., 2014. Geomorphic response of submarine canyons to tectonic activity: Insights from the Cook Strait canyon system, New Zealand. Geosphere 10, 905–929. https://doi.org/10.1130/GES01040.1

Miller, K.G., Mountain, G.S., 1996. Drilling and Dating New Jersey Oligocene-Miocene Sequences: Ice Volume, Global Sea Level, and Exxon Records. Science 271, 1092–1095. https://doi.org/10.1126/science.271.5252.1092

Miller, K.G., Mountain, G.S., Browning, J.V., Kominz, M., Sugarman, P.J., Christie-Blick, N., Katz, M.E., Wright, J.D., 1998. Cenozoic global sea level, sequences, and the New Jersey Transect: Results From coastal plain and continental slope drilling. Reviews of Geophysics 36, 569–601. https://doi.org/10.1029/98RG01624

Moore, G.F., Aung, L.T., Fukuchi, R., Sample, J.C., Hellebrand, E., Kopf, A., Naing, W., Than, W.M., Tun, T.N., 2019. Tectonic, diapiric and sedimentary chaotic rocks of the Rakhine coast, western Myanmar. Gondwana Research, Mélanges: 100th anniversary of the inception of the term and concept 74, 126–143. https://doi.org/10.1016/j.gr.2019.04.006

Moore, G.F., Boston, B.B., Strasser, M., Underwood, M.B., Ratliff, R.A., 2015. Evolution of tectono-sedimentary systems in the Kumano Basin, Nankai Trough forearc. Marine and Petroleum Geology 67, 604–616. https://doi.org/10.1016/j.marpetgeo.2015.05.032

Mountjoy, J.J., Barnes, P.M., Pettinga, J.R., 2009. Morphostructure and evolution of submarine canyons across an active margin: Cook Strait sector of the Hikurangi Margin, New Zealand. Marine Geology 260, 45–68. https://doi.org/10.1016/j.margeo.2009.01.006

Mulder, T., Callec, Y., Parize, O., Joseph, P., Schneider, J.-L., Robin, C., Dujoncquoy, E., Salles, T., Allard, J., Bonnel, C., Ducassou, E., Etienne, S., Ferger, B., Gaudin, M., Hanquiez, V., Linares, F., Marchès, E., Toucanne, S., Zaragosi, S., 2010. High-resolution analysis of submarine lobes deposits: Seismic-scale outcrops of the Lauzanier area (SE Alps, France). Sedimentary Geology, Lobes in deep-sea turbidite systems 229, 160–191. https://doi.org/10.1016/j.sedgeo.2009.11.005

Mulder, T., Syvitski, J.P.M., Migeon, S., Faugères, J.-C., Savoye, B., 2003. Marine hyperpycnal flows: initiation, behavior and related deposits. A review. Marine and Petroleum Geology, Turbidites: Models and Problems 20, 861–882. https://doi.org/10.1016/j.marpetgeo.2003.01.003

1188 Mullins, H.T., Keller, G.H., Kofoed, J.W., Lambert, D.N., Stubblefield, W.L., Warme, J.E., 1982.
1189 Geology of Great Abaco Submarine Canyon (Blake Plateau): Observations from the research
1190 submersible "Alvin." Marine Geology 48, 239–257. https://doi.org/10.1016/0025-
1191 3227(82)90099-8
1192 Mutti, E., Tinterri, R., Benevelli, G., Biase, D. di, Cavanna, G., 2003. Deltaic, mixed and turbidite
1193 sedimentation of ancient foreland basins. Marine and Petroleum Geology, Turbidites: Models
1194 and Problems 20, 733–755. https://doi.org/10.1016/j.marpetgeo.2003.09.001
1195 Nelson, C.H., Escutia, C., Damuth, J.E., Twichell, D.C., Jr., 2011. Interplay of Mass-Transport and
1196 Turbidite-System Deposits in Different Active Tectonic and Passive Continental Margin
1197 Settings: External and Local Controlling Factors, in: Shipp, R.C., Weimer, P., Posamentier, H.W.
1198 (Eds.), Mass-Transport Deposits in Deepwater Settings. SEPM Society for Sedimentary
1199 Geology, p. 0. https://doi.org/10.2110/sepmsp.096.039
1200 Normark, W.R., Carlson, P.C., 2003. Giant submarine canyons: Is size any clue to their importace in
1201 rock record ? GSA Bulletin 370, 1–15.
1202 Odonne, F., Callot, P., Debroas, E.-J., Sempere, T., Hoareau, G., Maillard, A., 2011. Soft-sediment
1203 deformation from submarine sliding: Favourable conditions and triggering mechanisms in
1204 examples from the Eocene Sobrarbe delta (Ainsa, Spanish Pyrenees) and the mid-Cretaceous
1205 Ayabacas Formation (Andes of Peru). Sedimentary Geology, Recognising triggers for soft-
1206 sediment deformation: Current understanding and future directions 235, 234–248.
1207 https://doi.org/10.1016/j.sedgeo.2010.09.013
1208 Ogata, K., Festa, A., Pini, G.A., Pogačnik, Ž., Lucente, C.C., 2019. Substrate deformation and
1209 incorporation in sedimentary mélanges (olistostromes): Examples from the northern Apennines
1210 (Italy) and northwestern Dinarides (Slovenia). Gondwana Research, Mélanges: 100th
1211 anniversary of the inception of the term and concept 74, 101–125.
1212 https://doi.org/10.1016/j.gr.2019.03.001
1213 Olsson, R.K., Berggren, W.A., Hemleben, C., Huber, B.T., 1999. Atlas of Paleocene planktonic
1214 foraminifera, Smithsonian Contributions to Paleobiology, **85**, 1–252,
1215 https://doi.org/10.5479/si.00810266.85.1.
1216 Orange, D.L., Breen, N.A., 1992. The effects of fluid escape on accretionary wedges 2. Seepage force,
1217 slope failure, headless submarine canyons, and vents. Journal of Geophysical Research: Solid
1218 Earth 97, 9277–9295. https://doi.org/10.1029/92JB00460
1219 Pairis, J.L., 1971. Tectonique et sédimentation tertiaire sur la marge orientale du bassin de Barrème
1220 (Alpes de Haute-Provence). Géologie Alpine 203–214.
1221 Park, Y., Yoo, D., Kang, N., Yi, B., 2019. Origin and Evolution of Stacked Cut-and-fill Structures On
1222 the Southwestern Margin of the Ulleung Basin, East Sea (Japan Sea). Journal of Sedimentary
1223 Research 89, 679–700. https://doi.org/10.2110/jsr.2019.36
1224 Paull, C.K., Caress, D.W., Lundsten, E., Gwiazda, R., Anderson, K., McGann, M., Conrad, J., Edwards,
1225 B., Sumner, E.J., 2013. Anatomy of the La Jolla Submarine Canyon system; offshore southern
1226 California. Marine Geology 335, 16–34. https://doi.org/10.1016/j.margeo.2012.10.003
1227 Paull, C.K., Freeman-Lynde, R., Bralower, T.J., Gardemal, J.M., Neumann, A.C., D'Argenio, B.,
1228 Marsella, E., 1990a. Geology of the strata exposed on the Florida Escarpment. Marine Geology
1229 91, 177–194. https://doi.org/10.1016/0025-3227(90)90035-I
1230 Paull, C.K., Spiess, F.N., Curray, J.R., Twichell, D.C., 1990b. Origin of Florida Canyon and the role of
1231 spring sapping on the formation of submarine box canyons. GSA Bulletin 102, 502–515.
1232 https://doi.org/10.1130/0016-7606(1990)102<0502:OOFCAT>2.3.CO;2
1233 Pearson, P.N., Olsson, R.K., Huber, B.T., Hemleben, C., Berggren, W.A., 2006. Atlas of Eocene
1234 planktonic foraminifera, Cushman Foundation for Foraminiferal Research, Pec. Publ. **41**, 1–513,
1235 Fredericksburg, USA.

Pekar, S., Miller, K.G., 1996. New Jersey Oligocene "Icehouse" sequences (ODP Leg 150X) correlated with global δ18O and Exxon eustatic records. Geology 24, 567–570. https://doi.org/10.1130/0091-7613(1996)024<0567:NJOISO>2.3.CO;2

Pekar, S.F., Christie-Blick, N., Kominz, M.A., Miller, K.G., 2002. Calibration between eustatic estmates from backstripping and oxygen isotopic records for the Oligocene. Geology 30, 903–906.

Pekar, S.F., Hucks, A., Fuller, M., Li, S., 2005. Glacioeustatic changes in the early and middle Eocene (51–42 Ma): Shallow-water stratigraphy from ODP Leg 189 Site 1171 (South Tasman Rise) and deep-sea δ18O records. GSA Bulletin 117, 1081–1093. https://doi.org/10.1130/B25486.1

Pekar, S.F., Miller, K.G., Kominz, M.A., 2000. Reconstructing the stratal geometry of latest Eocene to Oligocene sequences in New Jersey: resolving a patchwork distribution into a clear pattern of progradation. Sedimentary Geology 134, 93–109. https://doi.org/10.1016/S0037-0738(00)00015-4

Perch-Nielsen, K., 1985. Cenozoic calcareous nannofossils, in: Plankton Stratigraphy. Cambridge University Press, pp. 427–555.

Petrizzo, M.R., Premoli Silva, I., Verga, I., 2011. Practical Manual of Cretaceous Planktonic Foraminifera. International School on Planktonic Foraminifera, 3rd Course 2004, New Editing 2011, University of Perugia. ed. Universities of Perugia, Perugia.

Pochat, S., Van Den Driessche, J., 2007. Impact of synsedimentary metre-scale normal fault scarps on sediment gravity flow dynamics: An example from the Grès d'Annot Formation, SE France. Sedimentary Geology 202, 796–820. https://doi.org/10.1016/j.sedgeo.2007.09.005

Posamentier, H.W., Erskine, R.D., Mitchum, R.M.Jr., 1991. Models for Submarine-Fan Deposition within a Sequence-Stratigraphic Framework, in: Seismic Facies and Sedimentary Processes of Submarine Fans and Turbidite Systems, Frontiers in Sedimentary Geology. Springer, New York, NY, pp. 127–136. https://doi.org/10.1007/978-1-4684-8276-8_6

Pratson, L.F., Coakley, B.J., 1996. A model for the headward erosion of submarine canyons induced by downslope-eroding sediment flows. Geological Society of America Bulletin 108, 225–234.

Pratson, L.F., Nittrouer, C.A., Wiberg, P.L., Steckler, M.S., Swenson, J.B., Cacchione, D.A., Karson, J.A., Murray, A.B., Wolinsky, M.A., Gerber, T.P., Mullenbach, B.L., Spinelli, G.A., Fulthorpe, C.S., O'grady, D.B., Parker, G., Driscoll, N.W., Burger, R.L., Paola, C., Orange, D.L., Field, M.E., Friedrichs, C.T., Fedele, J.J., 2007. Seascape Evolution on Clastic Continental Shelves and Slopes, in: Continental Margin Sedimentation : From Sediment Transport to Sequence Stratigraphy, International Association of Sedimentologists Special Publication. John Wiley & Sons, Ltd, pp. 339–380. https://doi.org/10.1002/9781444304398.ch7

Pratson, L.F., Ryan, W.B.F., Mountain, G.S., Twichell, D.C., 1994. Submarine canyon initiation by downslope-eroding sediment flows: Evidence in late Cenozoic strata on the New Jersey continental slope. GSA Bulletin 106, 395–412. https://doi.org/10.1130/0016-7606(1994)106<0395:SCIBDE>2.3.CO;2

Rasmussen, E.S., 1994. The relationship between submarine canyon fill and sea-level change: an example from Middle Miocene offshore Gabon, West Africa. Sedimentary Geology 90, 61–75. https://doi.org/10.1016/0037-0738(94)90017-5

Ratzov, G., Sosson, M., Collot, J.-Y., Migeon, S., 2012. Late Quaternary geomorphologic evolution of submarine canyons as a marker of active deformation on convergent margins: The example of the South Colombian margin. Marine Geology 315–318, 77–97. https://doi.org/10.1016/j.margeo.2012.05.005

Ravenne, C., Vially, R., Riché, P., Trémolières, P., 1987. Sédimentation et tectonique dans le bassin marin Éocène supérieur-Oligocène des Alpes du Sud. Revue de l'Institut Français du Pétrole 42, 529–553.

Robert, K., Jones, D.O.B., Tyler, P.A., Van Rooij, D., Huvenne, V.A.I., 2015. Finding the hotspots within a biodiversity hotspot: fine-scale biological predictions within a submarine canyon using

high-resolution acoustic mapping techniques. Marine Ecology 36, 1256–1276. https://doi.org/10.1111/maec.12228

Rothwell, R.G., Thomson, J., Kähler, G., 1998. Low-sea-level emplacement of a very large Late Pleistocene 'megaturbidite' in the western Mediterranean Sea. Nature 392, 377–380. https://doi.org/10.1038/32871

Ryan, W., Cita, M., Miller, E.R., Hanselman, D.F., Nesteroff, W., Hecker, B., Nibbelink, M.F., 1978. Bedrock geology in new england submarine canyons. Ocean Acta 1, 233–254.

Schettino, A., Scotese, C.R., 2002. Clobal kinematic constraints to the tectonic evolution of the western Mediterranean since the Oligocene, in: Reconstitution of the Evolution of the Alpine-Himalayan Orogeny. Journal of the Virtual Explorer, 2002.

Schmid, S.M., Pfiffner, O.A., Froitzheim, N., Schönborn, G., Kissling, E., 1996. Geophysical-geological transect and tectonic evolution of the Swiss-Italian Alps. Tectonics 15, 1036–1064. https://doi.org/10.1029/96TC00433

Seidler, L., 2000. Incised submarine canyons governing new evidence of Early Triassic rifting in East Greenland. Palaeogeography, Palaeoclimatology, Palaeoecology 161, 267–293. https://doi.org/10.1016/S0031-0182(00)00126-7

Shepard, F.P., 1981. Submarine Canyons: Multiple Causes and Long-Time Persistence. AAPG Bulletin 65, 1062–1077. https://doi.org/10.1306/03B59459-16D1-11D7-8645000102C1865D

Shepard, F.P., 1972. Submarine canyons. Earth-Science Reviews 8, 1–12. https://doi.org/10.1016/0012-8252(72)90032-3

Shepard, F.P., Dill, R.F., 1966. Submarine canyons and other sea valleys. Rand McNally Comp., Chicago.

Sinclair, H.D., 1994. The influence of lateral basinal slopes on turbidite sedimentation in the Annot sandstones of SE France. Journal of Sedimentary Research 64, 42–54. https://doi.org/10.1306/D4267CFD-2B26-11D7-8648000102C1865D

Sobiesiak, M.S., Kneller, B., Alsop, G.I., Milana, J.P., 2016. Internal deformation and kinematic indicators within a tripartite mass transport deposit, NW Argentina. Sedimentary Geology, The environmental significance of soft-sediment deformation 344, 364–381. https://doi.org/10.1016/j.sedgeo.2016.04.006

Soulet, Q., Migeon, S., Gorini, C., Rubino, J.-L., Raisson, F., Bourges, P., 2016. Erosional versus aggradational canyons along a tectonically-active margin: The northeastern Ligurian margin (western Mediterranean Sea). Marine Geology 382, 17–36. https://doi.org/10.1016/j.margeo.2016.09.015

Speijer, R.P., Pälike, H., Hollis, C.J., Hooker, J.J., Ogg, J.G., 2020. Chapter 28 - The Paleogene Period, in: Gradstein, F.M., Ogg, James G., Schmitz, M.D., Ogg, G.M. (Eds.), Geologic Time Scale 2020. Elsevier, pp. 1087–1140. https://doi.org/10.1016/B978-0-12-824360-2.00028-0

Stanley, D.J., 1961. Études sédimentologiques des Grès d'Annot et de leurs équivalents latéraux (Thèse de doctorat en Sciences Naturelles). Université de Grenoble.

Sztrákos, K., du Fornel, E., 2003. Stratigraphie, paléoécologie et foraminifères du paléogène des Alpes Maritimes et des Alpes de Haute-Provence (Sud-Est de la France). 46 229–267.

Tempier, C., 1979. Plis et chevauchements dans la couverture sédimentaire autochtone secondaire et tertiaire des Alpes-Maritimes. Relations avec le comportement dishamonique de la couverture. C. R. Acad. Sc. Paris 288 (8 janiver 1979), série D, 39–41.

Trotter, J.A., Pattiaratchi, C., Montagna, P., Taviani, M., Falter, J., Thresher, R., Hosie, A., Haig, D., Foglini, F., Hua, Q., McCulloch, M.T., 2019. First ROV Exploration of the Perth Canyon: Canyon Setting, Faunal Observations, and Anthropogenic Impacts. Frontiers in Marine Science 6.

Vail, P.R., Audemard, F., Bowman, S.A., Eisner, P.N., Perez-Cruz, C., 1991. The Stratigraphic Signatures of Tectonics, Eustasy and Sedimentology - an Overview, in: Cycles and Events in Stratigraphy. Springer-Verlag, Berlin Heidelberg, pp. 617–659.

1335 Vinnels, J.S., Butler, R.W.H., McCaffrey, W.D., Lickorish, W.H., 2010. Sediment Distribution and
1336 Architecture Around a Bathymetrically Complex Basin: An Example from the Eastern
1337 Champsaur Basin, Se France. Journal of Sedimentary Research 80, 216–235.
1338 https://doi.org/10.2110/jsr.2010.025
1339 Wade, B.S., Olsson, R.K., Pearson, P.N., Huber, B.T., Berggren, W.A., 2018. Atlas of Oligocene
1340 Planktonic Foraminifera, Cushman Foundation for Foraminiferal Research, Spec. Publ.
1341 Cushman Foundation for Foraminiferal Research. Cushman Foundation for Foraminiferal
1342 Research, Spec. Publ. **46**, 1–528.
1343 Wang, D., Wu, S., Yao, G., Lü, F., Strasser, M., 2014. Analysis of Quaternary Mass Transport Deposits
1344 Based on Seismic Data in Southern Deep-Water Region of Qiongdongnan Basin, South China
1345 Sea, in: Sassa, K., Canuti, P., Yin, Y. (Eds.), Landslide Science for a Safer Geoenvironment.
1346 Springer International Publishing, Cham, pp. 575–581. https://doi.org/10.1007/978-3-319-
1347 04996-0_88
1348 Wu, N., Nugraha, H.D., Zhong, G., Steventon, M.J., 2022. The role of mass-transport complexes in the
1349 initiation and evolution of submarine canyons. Sedimentology 69, 2181–2202.
1350 https://doi.org/10.1111/sed.12987
1351 Zecchin, M., Caffau, M., 2020. Emergence of a submarine canyon, Crotone Basin, southern Italy. Marine
1352 and Petroleum Geology 114, 104204. https://doi.org/10.1016/j.marpetgeo.2019.104204
1353 Zecchin, M., Caffau, M., Roda, C., 2011. Relationships between high-magnitude relative sea-level
1354 changes and filling of a coarse-grained submarine canyon (Pleistocene, Ionian Calabria, Southern
1355 Italy). Sedimentology 58, 1030–1064. https://doi.org/10.1111/j.1365-3091.2010.01194.x
1356 Zernitz, E.R., 1932. Drainage Patterns and Their Significance. The Journal of Geology 40, 498–521.
1357
1358

Figure captions

Figure 1 (color). (A) Simplified geological map of the Southern French Alpine Foreland Basin (redrawn after Kerckhove and Monjuvent, 1980; Rouire et al., 1980a, 1980b; Rouire and Blanc, 1979), and location of Fig. 2. Paleocurrents data are from Joseph and Lomas (2004), Ravenne et al. (1987) and Vinnels et al. (2010). Abbreviations: A, Annot; Al, Allos; B, Barrême; Bar, Barcelonnette; Br, Braux; Bor, Bordighera; C, Contes; Cas, Castellane; D, Devoluy; EC, eastern Champsaur, GC, Grand Coyer; L, Lauzanier; M, Menton; MT, Mont Tournairet; QC, Quatre Cantons; PC, Peira Cava; SA, Saint-Antonin; SE, Saint-Etienne de Tinée; SR, Sanguinière-Restefond; TE, Trois Evêchés; TH, Trois Hommes, Tor, Tortissa; Tr, Triora; O, Orcières; V, Vintimiglia; WC, western Champsaur. (B) Schematic lithostratigraphic chart of the Southern Alpine Foreland Basin (modified from Joseph and Lomas, 2004 and Ravenne et al., 1987). (C) location of Fig. 1A within France and Italy.

Figure 2 (color). Simplified geological map of La Bonette-Restefond area which constitutes the northern part of Sanguinière-Restefond sub-basin, superimposed to IGN topographic map (modified after Bouroullec et al., 2004; Jean, 1985; Kerckhove et al., 1974). See Fig. 1 for location. Locations of Figs. 3, 5, and 9 are also shown.

Figure 3 (color). (A) Simplified geological map of the study area which exhibits La Bonette Canyon and its longitudinal control by the Colombart Structure (modified after Bouroullec et al., 2004; Jean, 1985; Kerckhove et al., 1974). See Fig. 2 for location. Locations of figs. 4, 6, 8E, 10 and 12 are also shown. Abbreviations of fault names: BF, Bergère Fault; THF, Trois Hommes Fault. (B) Structural reconstruction of a bathymetric Digital Terrain Model of the La Bonette area by the time of the incision of the Grès d'Annot Upper Erosion Surface. The axis of the La Bonette Canyon and the axis of its probable tributaries are illustrated, as well as the locations and transport directions of the six main MTDs affecting the canyon flanks during the deposition of the Schistes à Blocs Formation. Area of low confidence of the model are indicated by question-marks. Note that the range of depth indicated for this bathymetric reconstruction is much greater than it was for the real submarine erosion, which was about 700 m-deep in the study area (see Fig. 5 and Tab. 1 for more details).

Figure 4 (color). Outcrop of the western side of Col de l'Escuzier and Tête Ronde which is located in the central part of the study area. See Fig. 3 for location. (A) Uninterpreted panorama, picture is taken by drone. (B) Interpreted panorama showing the control of N80°E normal faults on the canyon cross-section profile, where the thalweg is asymmetric and bounded by F2 and F3. The thalweg exhibits an

1393 axial incision controlled by F2. F1 is clearly truncated by the GAUES and sealed by the Schistes Bruns
1394 Member, whereas F2 and F3 seem to be active during canyon-fill deposition. Abbreviations: BF, Bergère
1395 Fault; DKL1, Debrite Key Level 1; DKL2, Debrite Key Level 2; F0B corresponds to the fault "F3" of
1396 Pochat and Van Den Driessche, 2007; GAUES, Grès d'Annot Upper Erosion Surface; THF, Trois
1397 Hommes Fault; w, width.
1398
1399 Figure 5 (color). Schematic cross-section of La Bonette Canyon and underlying Colombart Structure
1400 along the south-north direction, restored to Rupelian times, before the deposition of Schistes à Blocs
1401 Formation and the reactivation of F2, F3, Bergère Fault and Trois Hommes Fault (location in Fig. 2). A
1402 dip value of ten degrees toward the north has been subtracted to measured dip values, which are
1403 illustrated in Figs. 2 and 3A. Modified after Jean, 1985.
1404
1405 Figure 6 (color). Outcrop of the western side of Col du Colombart which is located in the eastern part of
1406 the study area. See Fig. 3 for location. (A) Uninterpreted panorama, picture is taken by drone. (B)
1407 Interpreted panorama showing the control of N80°E normal faults on the canyon cross-section profile.
1408 Tectonic activity of faults F2 and F3 continues during and/or after the infilling of the canyon by Schistes
1409 à Blocs Formation. The transport directions of MTDs 1 and 2, their lateral walls and internal structural
1410 blocks are illustrated. Locations of Figs. 7A, 7B, 7C and 7D are also indicated. Abbreviations: A.I., axial
1411 incision; Au, Autapie nappe; DKL1, Debrite Key Level 1; DKL2, Debrite Key Level 2; SB, Schistes
1412 Bruns Member.
1413
1414 Figure 7 (color). (A) Close-up view of the hectometric-high erosive wall controlled by F1b, the vertical
1415 offset of the fault is illustrated. See Fig. 6B for location. (B) Close-up view of a decametric-high erosive
1416 wall controlled by F1e which has at the most a metric vertical offset. Schistes Bruns Member is
1417 composed of thin bedded turbidites which onlap the erosive wall and are slumped few meters from the
1418 last toward the canyon axis. Purple dashed line is the facies variation between in place and slumped
1419 Schistes Bruns. Bedding is highlighted by white lines and slump decollements are illustrated by purple
1420 lines. See Fig. 6B for location. (C) Close-up view of a slide block of Grès d'Annot Formation reworked
1421 within the Schistes Bruns Member on the southern flank of the canyon. Olistolith bedding is illustrated
1422 by white and dashed lines and small internal thrusts are illustrated by pink and dashed lines. See Fig. 6B
1423 for location. (D) Close-up view of the northern sidewall of MTD2 which slightly thrusts the canyon-fill
1424 toward the north. Dimensions of orange card are 8 x 5 cm, geologist gives the scale for the background
1425 view. Deformed bedding of Grès d'Annot and Schistes Bruns is illustrated by white full and dashed
1426 lines. See Fig. 6B for location. Pink lines illustrate shear planes within deformed Schistes Bruns.

Figure 8 (color). Three types of elementary features which constitute the Grès d'Annot Upper Erosion Surface, which are erosive walls, ramps and terraces. Ramps cut thought at angles below 45°, terraces are subparallel to the underlying bedding, and walls are subvertical. The height of the erosive wall ranges from few centimeters to 90 m. Wall height depend on bedset(s) thickness and are not necessarily controlled by faults. (A) Smallest scale of crenulation we identified concerning the GAUES, which here constitutes steps with a height of few centimeters. (B) GAUES shaped by steps of few tens of centimeters. (C) Pluri-metric-high walls cutting through Grès d'Annot Fm at Pointe de Chaufrède. Walls are vertical and are affected by slumping during their scealing by Schistes Bruns. (D) Grès d'Annot Upper Erosion Surface locally covered by milli-metric thick surficial Fe-Mn hydroxide crust, the last is indicated by white dots on the largest picture which has been taken close to Cime de la Plate. Close-up view exhibits a particularly preserved encrustation which is onlapped by Schistes Bruns Member, dimensions of orange card are 8 x 5 cm. (E) Two erosive terraces separated by a pluri-metric high erosive ramp which slopes 10° to the east. (F) Successive erosive walls of pluri-decametric height which are not controlled by faults, along the outcrop of Barre de la Mauvaise Côte. The greatest wall is composed of two parts with different angles. Note that high walls and part of walls depend on the stratigraphy of sandstone sequences, which is illustrated by white dashed lines. Abbreviations: GAUES, Grès d'Annot Upper Erosion Surface; SaB Fm, Schistes à Blocs Formation ; SB Mbr, Schistes Bruns Member.

Figure 9 (color). Outcrop of the western side of Tête du Clot des Pastres which is located in the western part of the study area (modified after Mercier, 2022). See Fig. 2 for location. (A) Uninterpreted panorama, picture is taken by drone. (B) Interpreted panorama showing the control of N80°E normal faults on the canyon cross-section profile, but also the role of F5 on the location of MTD4 headscarp. MTD4 structural domains are also illustrated. Summits indicated by the prefix (i) are located in the foreground, (ii) in the middleground and (iii) in the background. Abbreviations: A.I., axial incision; Au, Autapie nappe; BF, Bergère Fault; Br, Briançonnais tectonic slices; CB; Cime de la Bonette; CBF, Caire Brun Fault; CC, Col de Colombart; CF, Chevalier Fault; CP, Cime de la Plate; DKL1, Debrite Key Level 1; DKL2, Debrite Key Level 2; GAUES, Grès d'Annot Upper Erosion Surface; GF, Gendron Fault; h, height; JF, Joubarde Fault; MF, Musique Fault; SBUES, Schistes Bruns Upper Erosion Surface; SCB, Sommet de Caire Brun; SRKL3, Shale-rich Key Level 3; TC, Tête de Cristel; TCP, Tête du Clot des Pastres; TG, Tête de Glaudon; THF, Trois Hommes Fault; TL, Tête du Lau; TR, Tête Ronde; TS, Tête de Sanguinière; w, width; Wf, wildflysch.

Figure 10 (color). (A) Uninterpreted picture taken by drone view of the outcrop from Col de Cime Plate to Baisse de la Plate, which is located in the western part of the study area. See Fig. 3A for location. (B) Interpreted picture taken by drone view of MTD5 which exhibits its northwestward oriented transport, the headscarp located close to the Bergère Fault, the evacuation zone (EZ) scealled by the Schistes à Blocs Fm, and the extensive and compressive domains. Note the absence of transition between the extensive and compressive domains. Abbreviations: BF, Bergère Fault; GAUES, Grès d'Annot Upper Erosion Surface.

Figure 11 (color). Wulff diagrams (lower hemisphere) showing faults plane orientations measured within MTDs 4 and 5 (modified after Mercier, 2022). The bending direction of the arcs indicates the direction of the fault dip, and arc edges indicate the strike direction of the fault plane. (A) normal faults of MTD4; (B) normal faults of MTD5; (C) internal shear zones of MTD4 which are all parallel to transport direction of the MTD; (D) internal shear zones of MTD5; (E) thrusts/reverse faults of MTD4; (F) thrusts/reverse faults of MTD5.

Figure 12 (color) (A) Interpreted picture taken by drone view of Baisse de la Plate Tributary, which is controlled by F6 and its antithetic fault F6b. See Fig. 3A for location. Note the numerous slide blocks of Annot Sandstones reworked within the Schistes à Blocs formation. Locations of Figs 12B and 12C are also shown. Abbreviation: GAUES, Grès d'Annot Upper Erosion Surface. (B) and (C) Highly deformed olistoliths of Grès d'Annot deposited within Schistes Bruns Member that fill-up the lower part of the Baisse de la Plate tributary. Purple dashed lines are decollement surface of slumped/fallen masses, pink lines and dashed lines are internal thrusts, brick-red lines and dashed lines are internal normal faults, and white lines and dashed lines illustrate the bedding of MTDs, turbidites of Schistes Bruns Member and canyon substratum.

Fig. 13. Separated biostratigraphic distribution of planktonic plus two benthic species of foraminifera and calcareous nannofossils recorded in the studied samples leading to their interpreted age (range in light grey according to foraminifera, in dark grey according to calcareous nannofossils), respectively. The orange interval corresponds to the most suitable age deduced for the Schistes Bruns and Schistes à Blocs Exotiques members (i.e. Schistes à Blocs Formation). Biozones according to Gradstein *et al*. (2020), the chronological distribution of species come from the Web resource https://www.mikrotax.org.

Figure 14 (color). (A) Geological time scale (after Gradstein et al., 2020). (B) Biostratigraphy of Neogene period showing biozones of planktonic foraminifera (Plank. Foram.), larger benthic

foraminifera (LBF) and calcareous nannofossils (Calc. Nanno.). Modified after Speijer *et al.* (2020). (C) Global eustatic curve during Paleogene period (modified after Miller et al., 2005). (D) $\delta^{18}O$ and $\delta^{13}C$ curves during Paleogene period and climatic events (*MECO*, Mid-Eocene Climatic Optimum; *PrOM*, Priabonian Oxygen Maximum; *EOT-1*, Eocene-Oligocene Transition; *Oi*-1 to *Oi-2b*, Oligocene $\delta^{18}O$ maxima/glacio-eustatic events. (E) Obliquity cycles of about 1,12 Ma during Oligocene causing 3rd order sequence boundaries and fitting with glacio-eustatic events (modified after Boulila et al., 2011). NP22-lower NP23 is the interpreted age of these deposits using the superposition principle with the Grès d'Annot formation, which is dated NP21 in the Sanguinière-Restefond Sub-basin (SRSB) by Sztrákos and du Fornel (2003). Note that the base of NP22 is marked by a 3rd order sequence boundary which has been highlighted in red for more convenance. Abbreviation: SRSB, Sanguinière-Restefond Sub-basin.

Figure 15 (color). Schematic diagram block showing the longitudinal control of La Bonette Canyon by the Colombart Structure, and its asymmetrical cross-section profile due to the asymmetry of the tectonic structure. Orientation of erosive features in the Lauzanier Sub-basin is less constrained and interpretated from 2D outcrop data after Mulder *et al.*, 2010. Abbreviations: BF, Bergère Fault; THF, Trois Hommes Fault.

Table 1. (A) Stratigraphic position (m) of the Grès d'Annot Upper Erosion surface within the different structural blocks of the Colombart Structure, in respect to the stratigraphic potision of Debrite Key Level 1. Stratigraphic data from logs made by Jean (1985) and from our own observations. The estimated vertical offsets of the normal faults of the Colombart Structure (location in Fig. 3A) are also indicated. Eastern values from Fig. 6, center values from Fig. 4 and western values from Fig. 9. Abbreviations: ftw, footwall ; g, graben ; h-g, half-graben, hgw, hanging wall, Twg, thalweg of La Bonette Canyon, Tête Sang., Tête de Sanguinière. (B) Calculated depth (m) of the Grès d'Annot Upper Erosion Surface within the Colombart Structure, taking in account the stratigraphic position of Tête de Sanguinière as reference (depth = 0 m) and substracting both stratigraphic values and the calculated Oligocene vertical offsets of faults indicated in Table 1A. Note that the substraction of vertical offsets deepens the thalweg of the La Bonette Canyon (740 m deep) by about 140 m from the value of 600 m indicated by Jean (1985), because of the structural control of the canyon by the normal faults which has been first pointed out by Lansigu (2000). The mean slope of each canyon flank is also estimated, showing that the northern flank is twice steeper than the southern flank. Abbreviations: ftw, footwall ; g, graben ; h-g, half-graben, hgw, hanging wall, Twg, thalweg of La Bonette Canyon, Tête Sang., Tête de Sanguinière.

Table 2. Heights of the largest submarine scarps identified within the study area and vertical offsets of controlling normal faults. The type of erosive feature(s) which constitute(s) the submarine scarp is detailed. The relative position of the scarp in respect to the structure (hanging wall or footwall) is also indicated.

Table 1 Suppl. Mat. Listing of the foraminifera and calcareous nannofossils recorded in the studied samples with their respective biostratigraphic range.

A	Vertical offsets of faults (m)		Canyon transverse profile	Position of Grès d'Annot Upper Erosion Surface (m) above Debrite Key Level 1		
				West (Fig. 9B)	Center (Fig. 4B)	East (Fig. 6B)
F1 ftw			North	200		250
F1	**during LBC excavation**	**100**		F1-F2 h-g : 30	F1-F2 h-g : 130	F1-F2 h-g : 200
	present	120				
F2	post GAUES (estimated)	40				F2-F3 g : 140 (20+120)
	during LBC excavation	**80**	Twg	F2-F4 h-g : 40		
F3	present	50+?				
F3	post GAUES (estimated)	50				
F4		?		F4-F5 horst : 40		
F5	**during LBC excavation**	**50**		F5-F6 h-g : 250		
F6	present	?				
F6 hgw				F6 hgw : 400		
Tête Sang.			South		600	

B	Vertical offsets of faults (m)		Canyon transverse profile	Depth of Grès d'Annot Upper Erosion Surface (m) compared to its stratigraphic position at Tete de Sanguinière, substracting known oligocene vertical offsets of faults		
				West	Center	East
F1 footwall			North	-400 (200-600)		-350 (250-600)
F1	**during LBC excavation**	**100**		-670 (30-600-100)	-570 (130-600-100)	-500 (200-600-100)
F2	present	120	mean slope = 19°			
F2	post GAUES (estimated)	40				**-640** (140-600-100-80)
F2	**during LBC excavation**	**80**	Twg	**-740** (40-600-100-80)		
F3	present	50+?				
F3	post GAUES (estimated)	50				
F4		?		-510 (40-600+50)		
F5	**during LBC excavation**	**50**		-350 (250-600)		
F6	present	?	mean slope = 10°			
F6 hanging wall				-200 (400-600)		
Tête Sang.			South		**0** (600-600)	

Controlling/guiding fault	Actual vertical offset of the fault	Late offset along the cited outcrop	Vertical offset during the Rupelian (*: late offset along the cited outcrop)	Block of the tectonic structure which is the most truncated by the GAUES	**Height of controlled/guided submarine scarp** (*:late offset of the controlling faut)	**Type of submarine scarp** (**: minor feature if composite scarp)	Figures
F1b	5 m	0 m	5 m	Footwall	**100 m**	Wall	7A
F2	120	40 m	120-40* = 80 m	Footwall	100-40* = 60 m	Wall	9B
F2	120	40 m	120-40* = 80 m	Footwall	160-40* = **120 m**	Wall and ramp**	9B
F2	120	20 m	120-20* = 100 m	Footwall	110-20* = **90 m**	Wall	9B
F0	unknown	unknown	unknown	Footwall	**150 m ?**	Wall	9B
CF (Chevalier Fault)	200 m	0 m	200 m	Footwall	**125 m**	Ramp and Wall**	9B
MF (Musique Fault)	200 m	0 m	200 m	Footwall	**90 m**	Wall	9B
CBF (Caire Brun Fault)	80 m	0 m	80 m	**Hanging wall**	70 m	Wall	9B
BF (Bergère Fault)	120 m	30 m	120-30* = 90 m	Footwall	300-30* = **270 m**	Wall	3A and 9B

Legend:

	Submarine scarp > 90 m-high controlled by a minor faut (small vertical offset during the Rupelian)
	Submarine scarp > 90 m-high controlled by a major faut (important vertical offset during the Rupelian)
	Submarine scarp > 50 m-high controlled by a major faut (important vertical offset during the Rupelian)

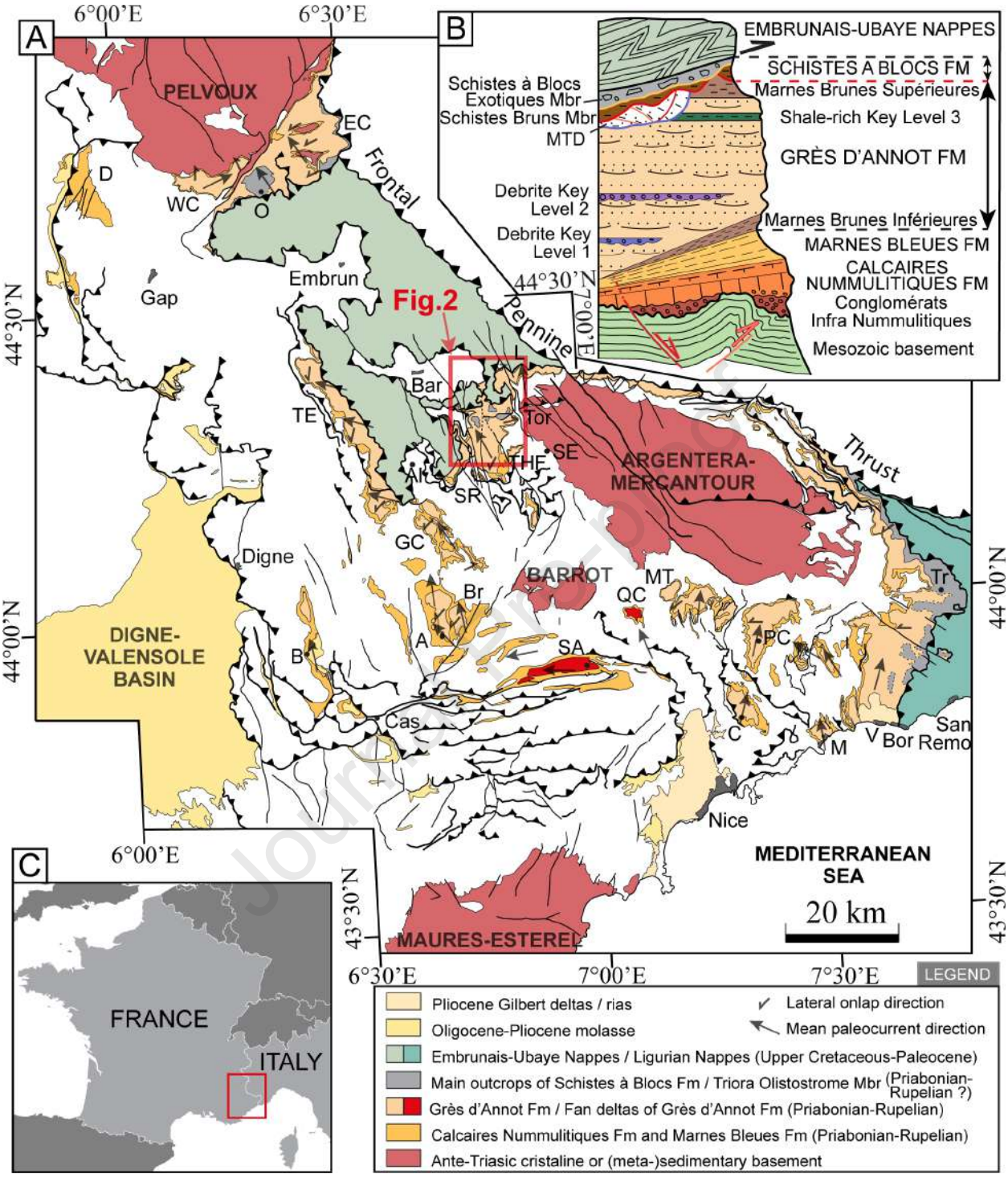
A
6°00'E
6°30'E
PELVOUX
EC
Frontal
D
WC
O
Gap
Embrun
Fig.2
Pennine
44°30'N
44°30'N
Bar
TE
Tor
SE
THE
AR
SR
ARGENTERA-
MERCANTOUR
Thrust
GC
Digne
BARROT
MT
QC
Br
A
B
SA
Tr
PC
DIGNE-
VALENSOLE
BASIN
Cas
C
M
V
Bor
San
Remo
Nice
MEDITERRANEAN
SEA
20 km
MAURES-ESTEREL
44°00'N
44°00'N
43°30'N
43°30'N
6°30'E
7°00'E
7°30'E
B
EMBRUNAIS-UBAYE NAPPES
SCHISTES A BLOCS FM
Schistes à Blocs
Exotiques Mbr
Schistes Bruns Mbr
MTD
Marnes Brunes Supérieures
Shale-rich Key Level 3
GRÈS D'ANNOT FM
Debrite Key
Level 2
Debrite Key
Level 1
Marnes Brunes Inférieures
MARNES BLEUES FM
CALCAIRES
NUMMULITIQUES FM
Conglomérats
Infra Nummulitiques
Mesozoic basement
C
6°00'E
FRANCE
ITALY
LEGEND
Pliocene Gilbert deltas / rias
Oligocene-Pliocene molasse
Embrunais-Ubaye Nappes / Ligurian Nappes (Upper Cretaceous-Paleocene)
Main outcrops of Schistes à Blocs Fm / Triora Olistostrome Mbr (Priabonian-Rupelian ?)
Grès d'Annot Fm / Fan deltas of Grès d'Annot Fm (Priabonian-Rupelian)
Calcaires Nummulitiques Fm and Marnes Bleues Fm (Priabonian-Rupelian)
Ante-Triasic cristaline or (meta-)sedimentary basement
Lateral onlap direction
Mean paleocurrent direction

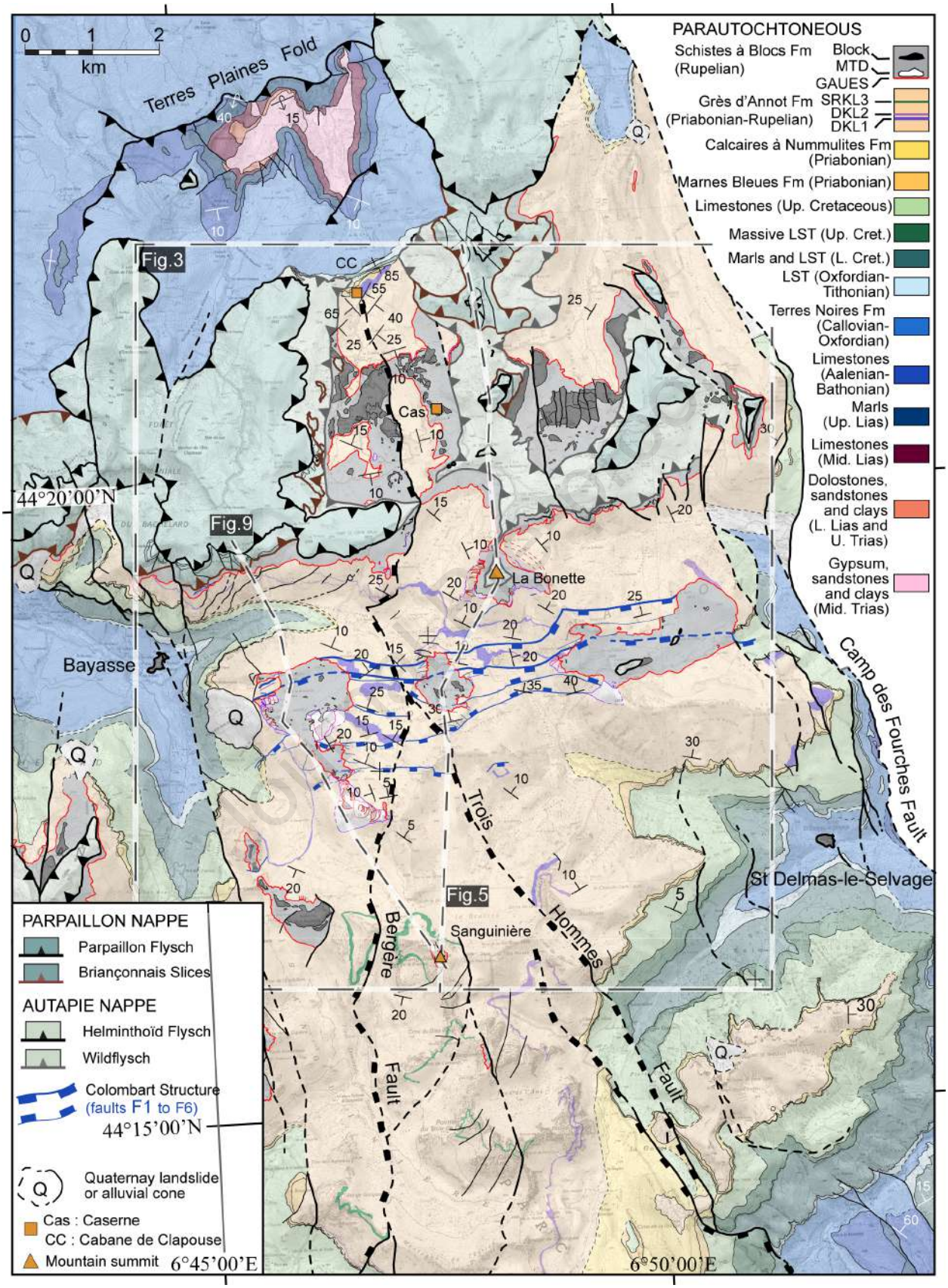
0 1 2
km
Terres Plaines Fold
Fig.3
Fig.9
Fig.5
CC
Cas
La Bonette
Sanguinière
Bayasse
St Delmas-le-Selvage
Camp des Fourches Fault
Trois Hommes Fault
Bergère Fault
44°20'00"N
44°15'00"N
6°45'00"E
6°50'00"E
PARAUTOCHTONEOUS
Schistes à Blocs Fm (Rupelian)
Block
MTD
GAUES
Grès d'Annot Fm (Priabonian-Rupelian)
SRKL3
DKL2
DKL1
Calcaires à Nummulites Fm (Priabonian)
Marnes Bleues Fm (Priabonian)
Limestones (Up. Cretaceous)
Massive LST (Up. Cret.)
Marls and LST (L. Cret.)
LST (Oxfordian-Tithonian)
Terres Noires Fm (Callovian-Oxfordian)
Limestones (Aalenian-Bathonian)
Marls (Up. Lias)
Limestones (Mid. Lias)
Dolostones, sandstones and clays (L. Lias and U. Trias)
Gypsum, sandstones and clays (Mid. Trias)
PARPAILLON NAPPE
Parpaillon Flysch
Briançonnais Slices
AUTAPIE NAPPE
Helminthoïd Flysch
Wildflysch
Colombart Structure (faults F1 to F6)
Quaternay landslide or alluvial cone
Cas : Caserne
CC : Cabane de Clapouse
Mountain summit

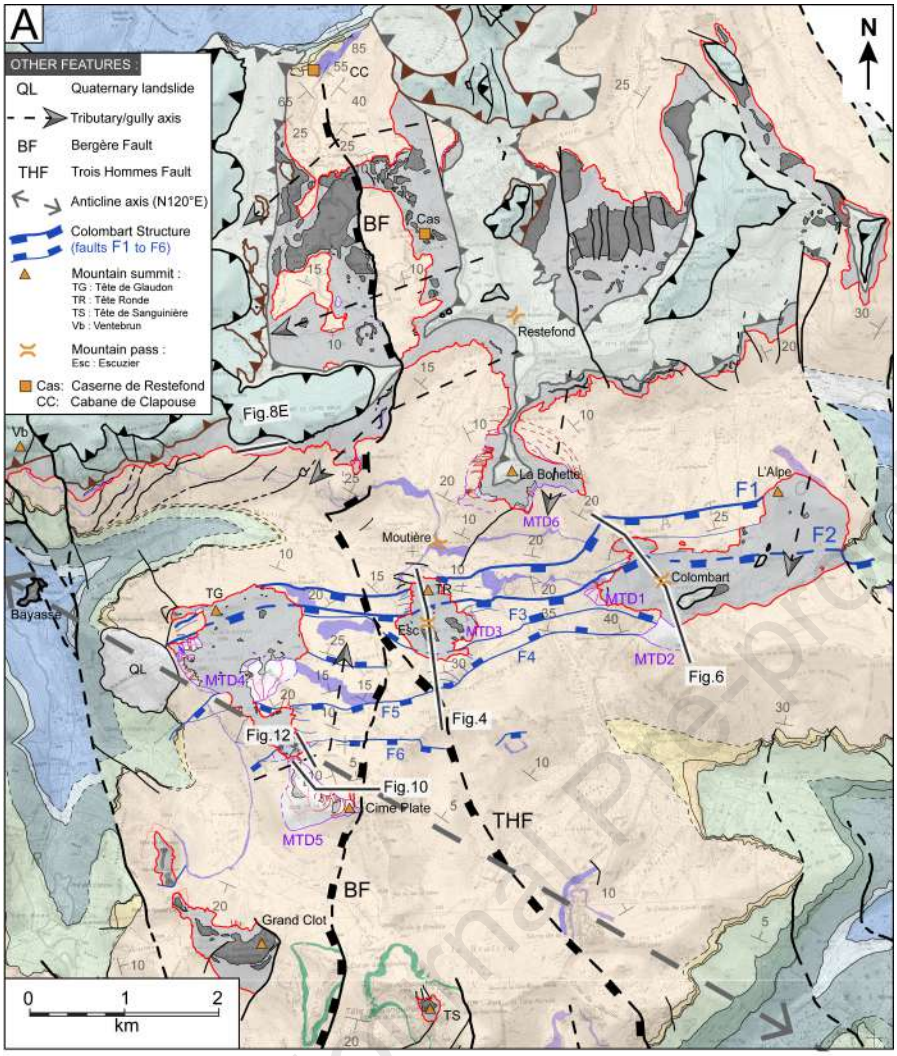

PARPAILLON NAPPE
- Parpaillon Flysch
- Briançonnais Slices

AUTAPIE NAPPE
- Helminthoïd Flysch
- Wildflysch

PARAUTOCHTONEOUS
- Block
- MTD
- **Schistes à Blocs Fm (Rupelian)**
- Grès d'Annot Upper Erosion Surface
- Shale-rich Key Level 3
- Debrite Key Level 2
- Debrite Key Level 1
- **Grès d'Annot Fm (Priabonian-Rupelian)**
- Calcaires à Nummulites Fm (Priabonian)
- Marnes Bleues Fm (Priabonian)

- Limestones (Upper Cretaceous)
- Massive limestones (Upper Cretaceous)
- Marls and limestones (Lower Cretaceous)
- Limestones (Oxfordian-Tithonian)
- Terres Noires Fm (Marls, Callovian-Oxfordian)

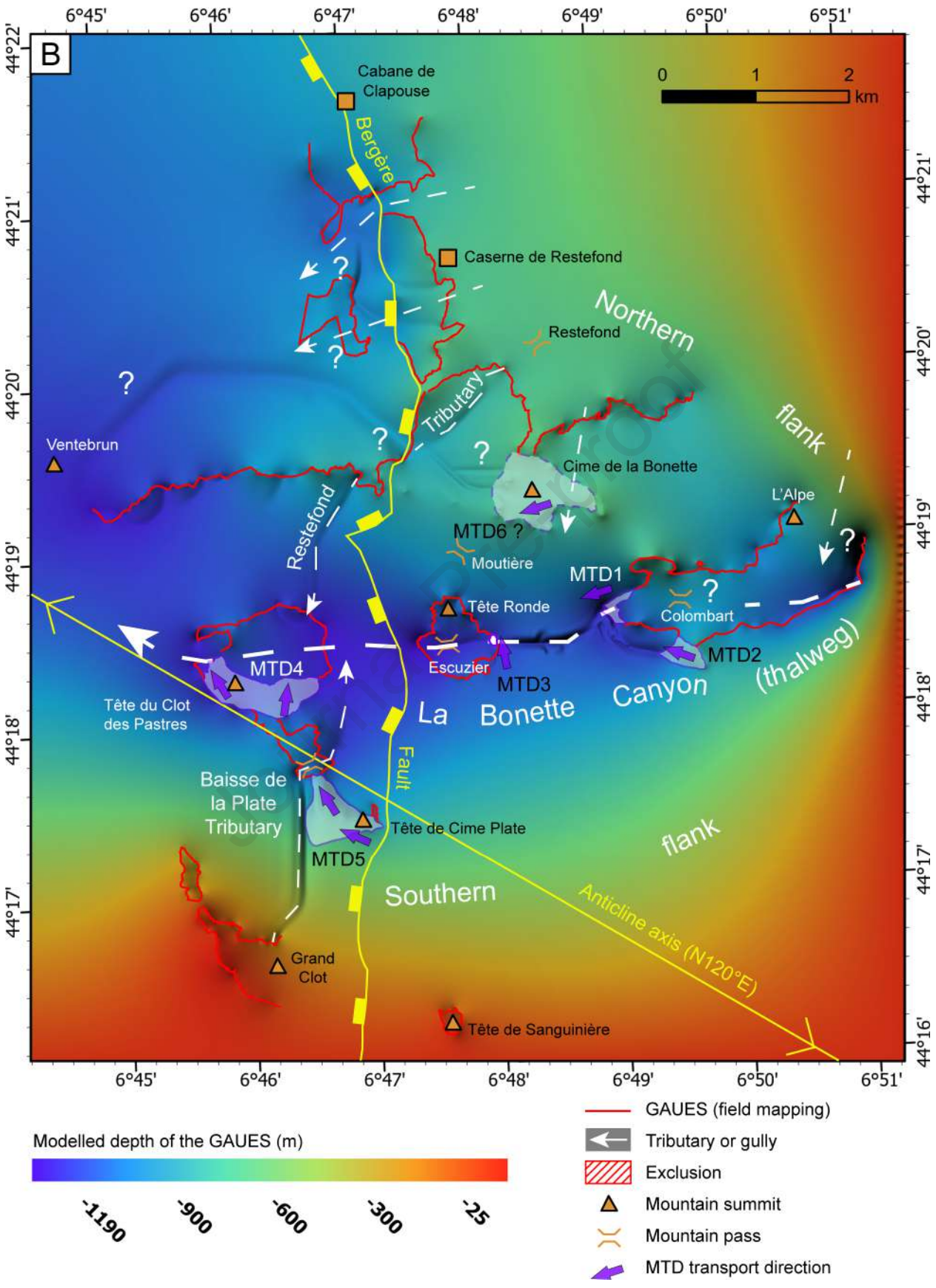
B
6°45'
6°46'
6°47'
6°48'
6°49'
6°50'
6°51'
44°22'
44°21'
44°20'
44°19'
44°18'
44°17'
44°16'
0
1
2
km
Cabane de Clapouse
Bergère
Caserne de Restefond
Restefond
Northern
Tributary
flank
Ventebrun
Restefond
Cime de la Bonette
L'Alpe
MTD6 ?
Moutière
MTD1
Tête Ronde
Colombart
Escuzier
MTD2
MTD3
MTD4
Canyon
(thalweg)
Tête du Clot des Pastres
La Bonette
Fault
Baisse de la Plate Tributary
Tête de Cime Plate
MTD5
flank
Southern
Anticline axis (N120°E)
Grand Clot
Tête de Sanguinière
Modelled depth of the GAUES (m)
-1190
-900
-600
-300
-25
GAUES (field mapping)
Tributary or gully
Exclusion
Mountain summit
Mountain pass
MTD transport direction

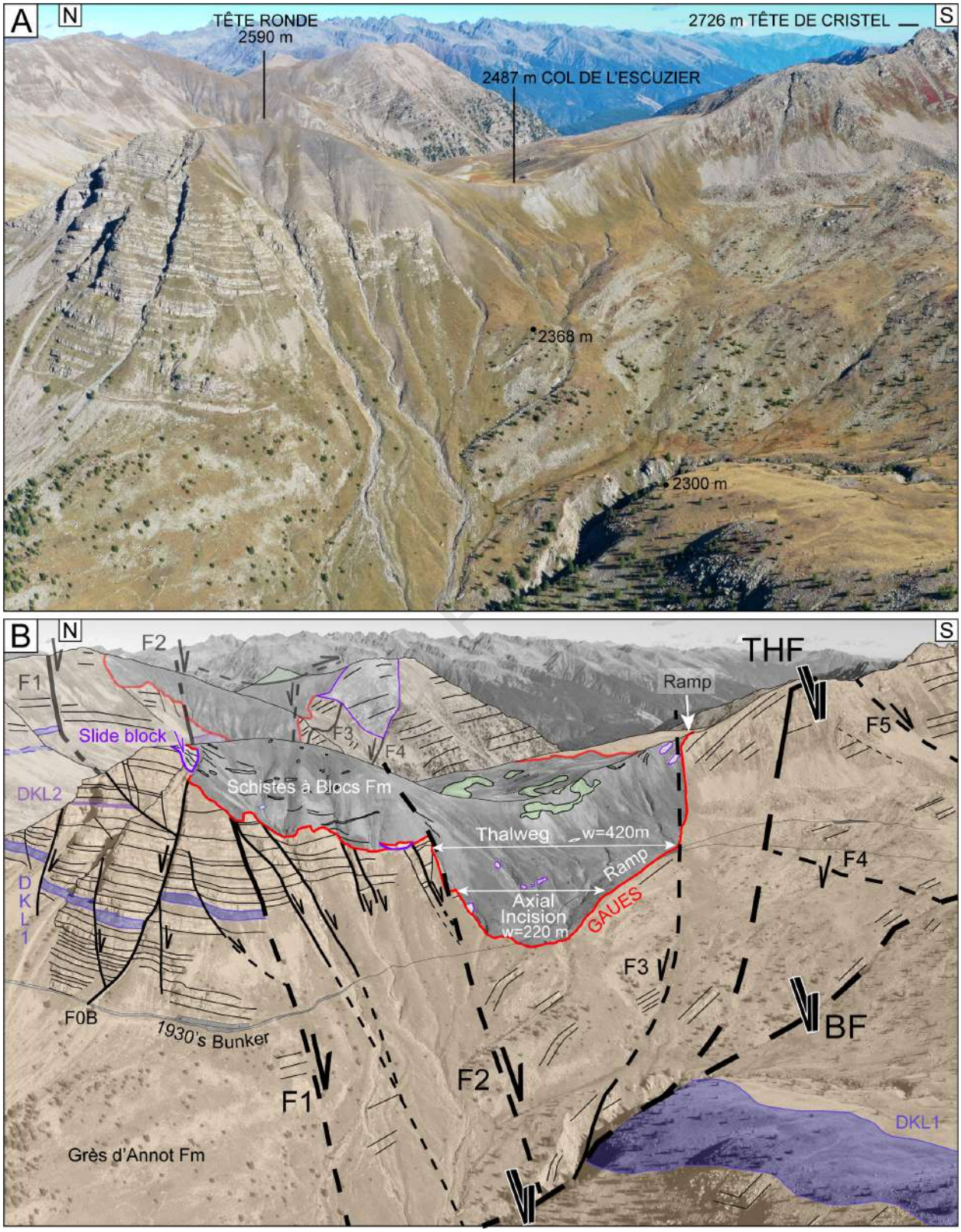
A
N
S
TÊTE RONDE
2590 m
2726 m TÊTE DE CRISTEL
2487 m COL DE L'ESCUZIER
2368 m
2300 m
B
N
S
F1
F2
F3
F4
F5
THF
Ramp
Slide block
DKL2
DKL1
Schistes à Blocs Fm
Thalweg
w=420m
Ramp
Axial
Incision
w=220 m
GAUES
F0B
1930's Bunker
BF
Grès d'Annot Fm

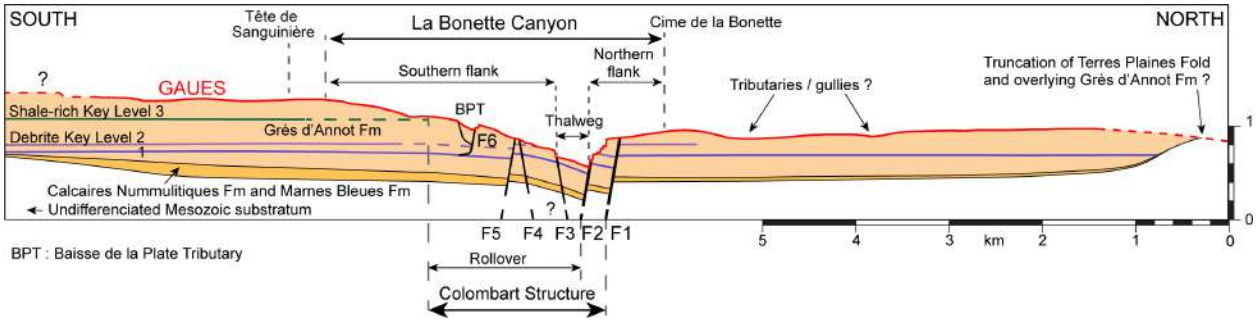

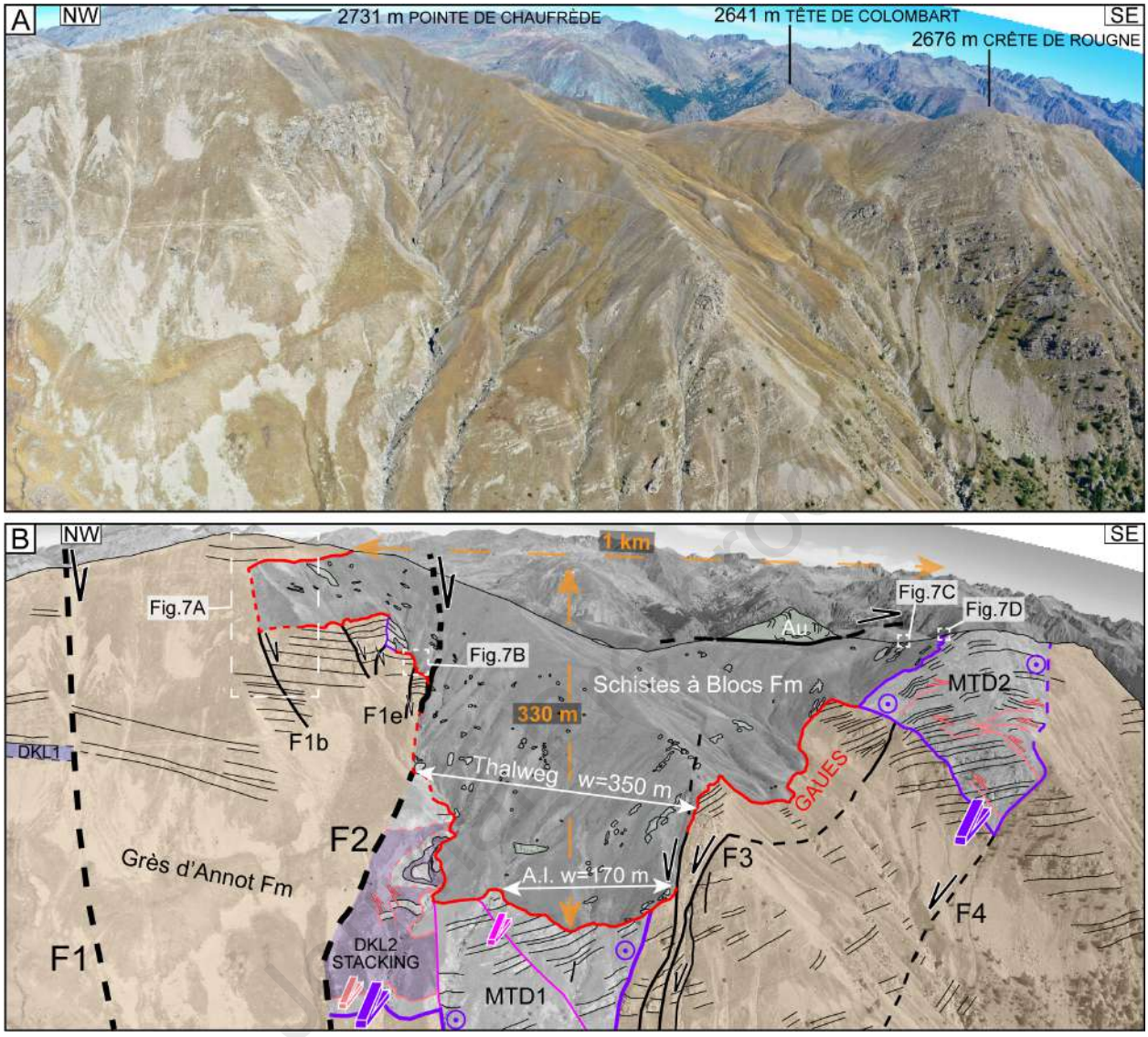
A
NW
2731 m POINTE DE CHAUFRÈDE
2641 m TÊTE DE COLOMBART
2676 m CRÊTE DE ROUGNE
SE
B
NW
SE
1 km
Fig.7A
Fig.7B
Fig.7C
Fig.7D
F1b
F1e
DKL1
330 m
Schistes à Blocs Fm
MTD2
Thalweg
w=350 m
GAUES
F2
F3
F4
Grès d'Annot Fm
A.I. w=170 m
F1
DKL2
STACKING
MTD1

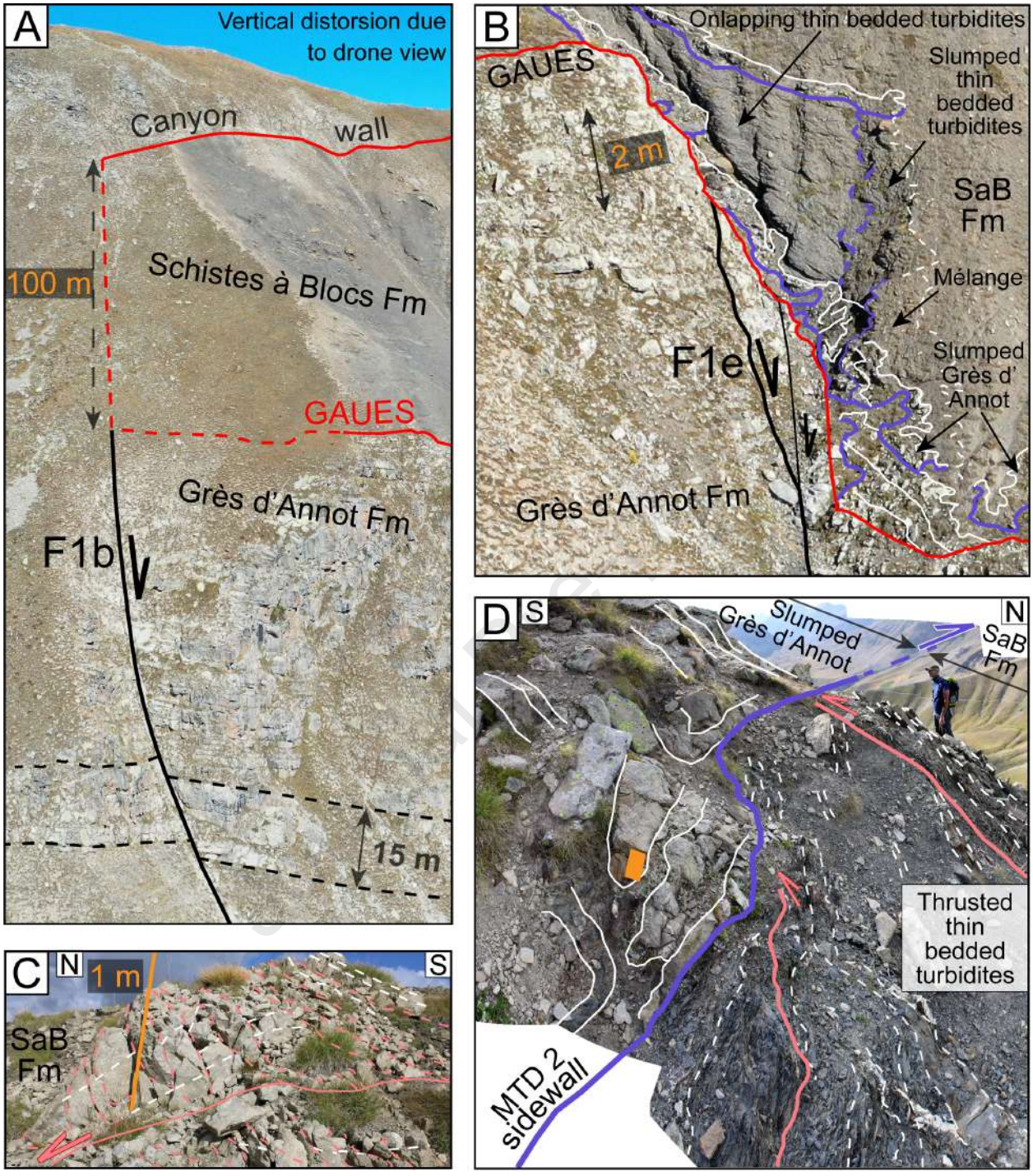
A
Vertical distorsion due to drone view
Canyon wall
100 m
Schistes à Blocs Fm
GAUES
Grès d'Annot Fm
F1b
15 m
B
Onlapping thin bedded turbidites
GAUES
2 m
Slumped thin bedded turbidites
SaB Fm
Mélange
F1e
Slumped Grès d' Annot
Grès d'Annot Fm
C
N
1 m
S
SaB Fm
D
S
Slumped Grès d'Annot
N
SaB Fm
Thrusted thin bedded turbidites
MTD 2 sidewall

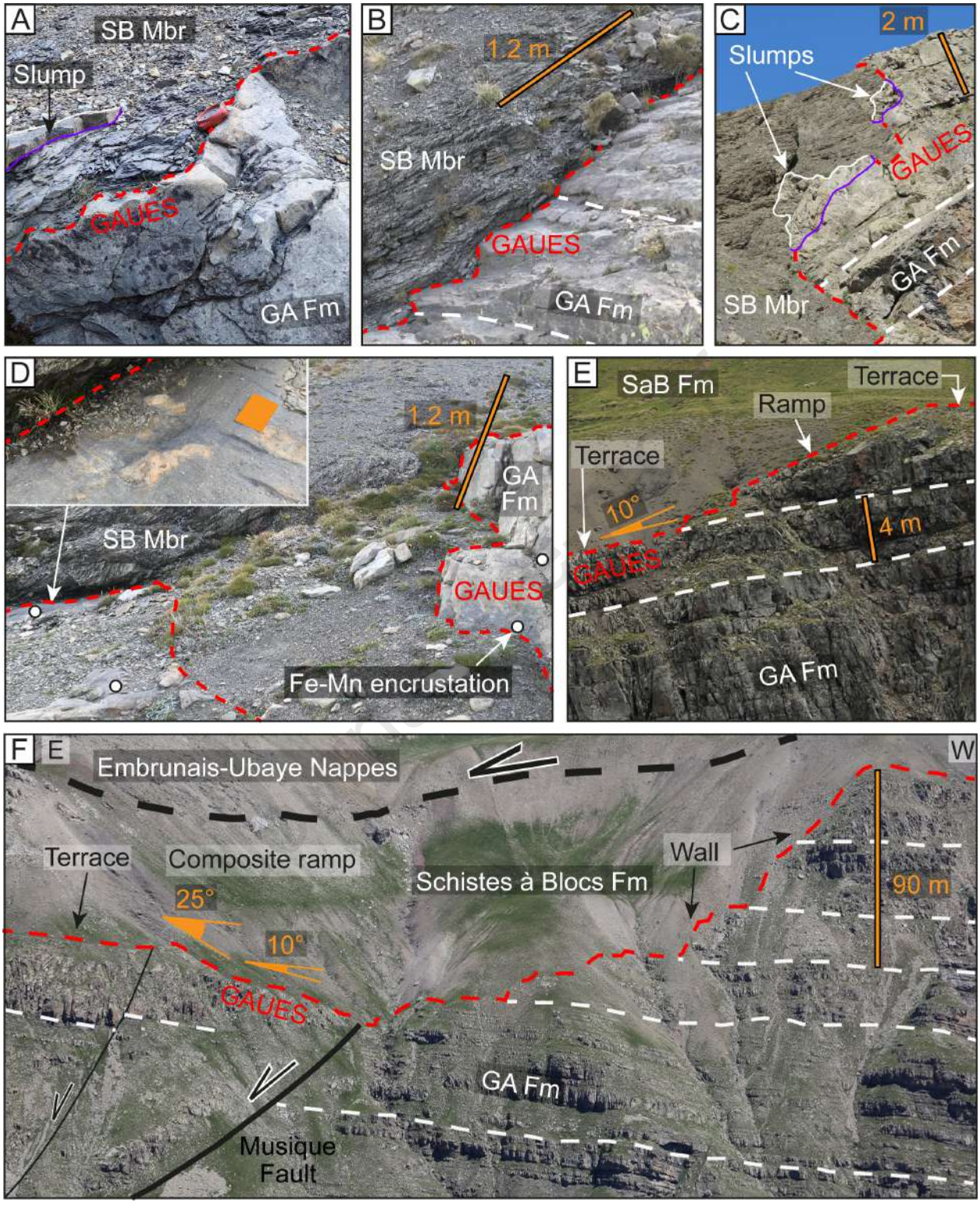
A
SB Mbr
Slump
GAUES
GA Fm
B
1.2 m
SB Mbr
GAUES
GA Fm
C
2 m
Slumps
GAUES
GA Fm
SB Mbr
D
1.2 m
GA Fm
SB Mbr
GAUES
Fe-Mn encrustation
E
SaB Fm
Terrace
Ramp
Terrace
10°
4 m
GAUES
GA Fm
F
E
W
Embrunais-Ubaye Nappes
Terrace
Composite ramp
25°
10°
GAUES
Schistes à Blocs Fm
Wall
90 m
GA Fm
Musique
Fault

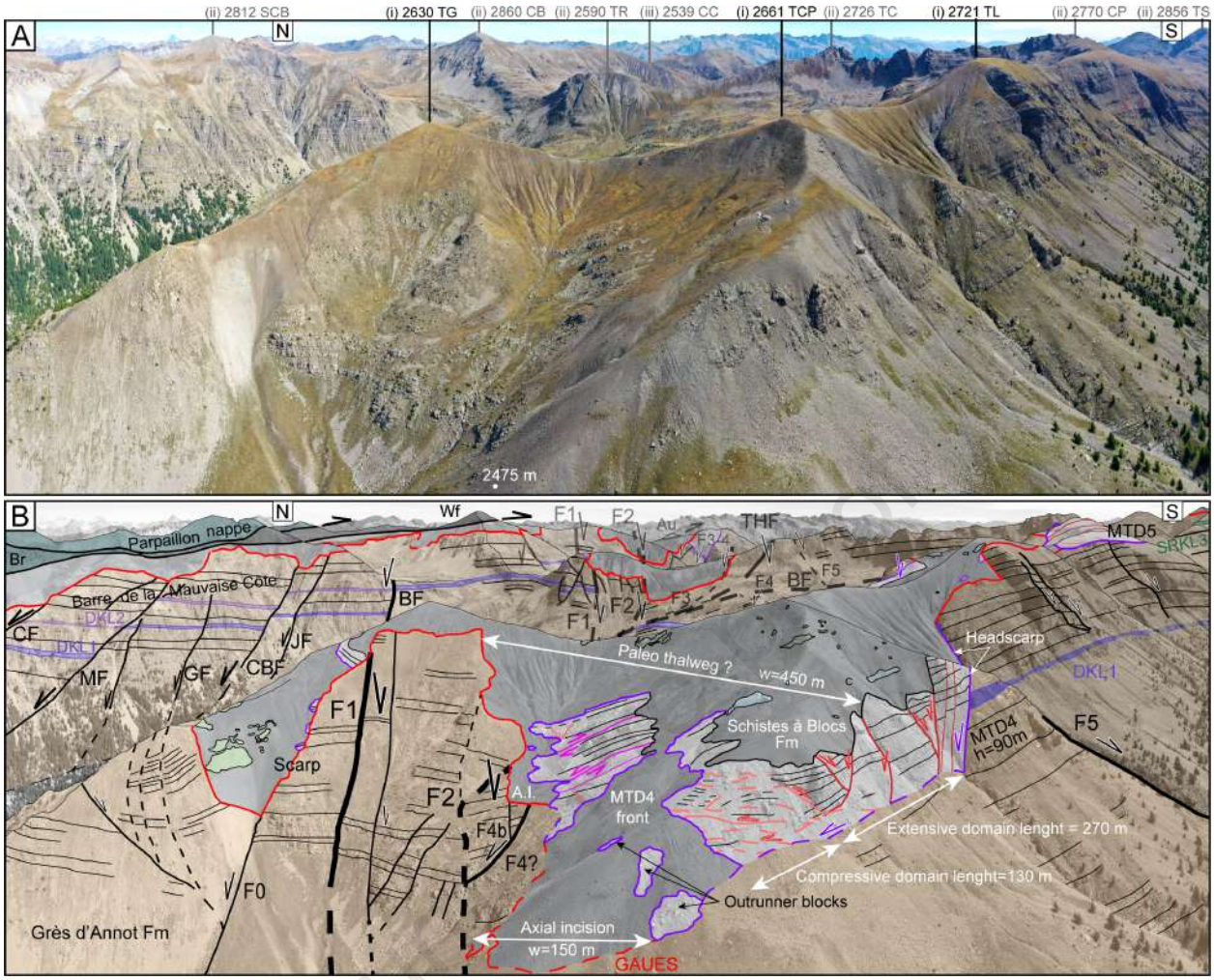
(ii) 2812 SCB
(i) 2630 TG
(ii) 2860 CB
(ii) 2590 TR
(iii) 2539 CC
(i) 2661 TCP
(ii) 2726 TC
(i) 2721 TL
(ii) 2770 CP
(ii) 2856 TS
A
N
S
2475 m
B
N
S
Wf
F1
F2
Au
F3/4
THF
F4
BF
F5
MTD5
SRKL3
Parpaillon nappe
Br
Barre de la Mauvaise Côte
DKL2
DKL1
CF
JF
MF
GF
CBF
F1
F2
F3
BF
Paleo thalweg ?
w=450 m
Headscarp
DKL1
Schistes à Blocs Fm
MTD4 h=90m
F5
Scarp
F1
F2
A.I.
F4b
F4?
F0
MTD4 front
Extensive domain lenght = 270 m
Compressive domain lenght=130 m
Outrunner blocks
Grès d'Annot Fm
Axial incision
w=150 m
GAUES

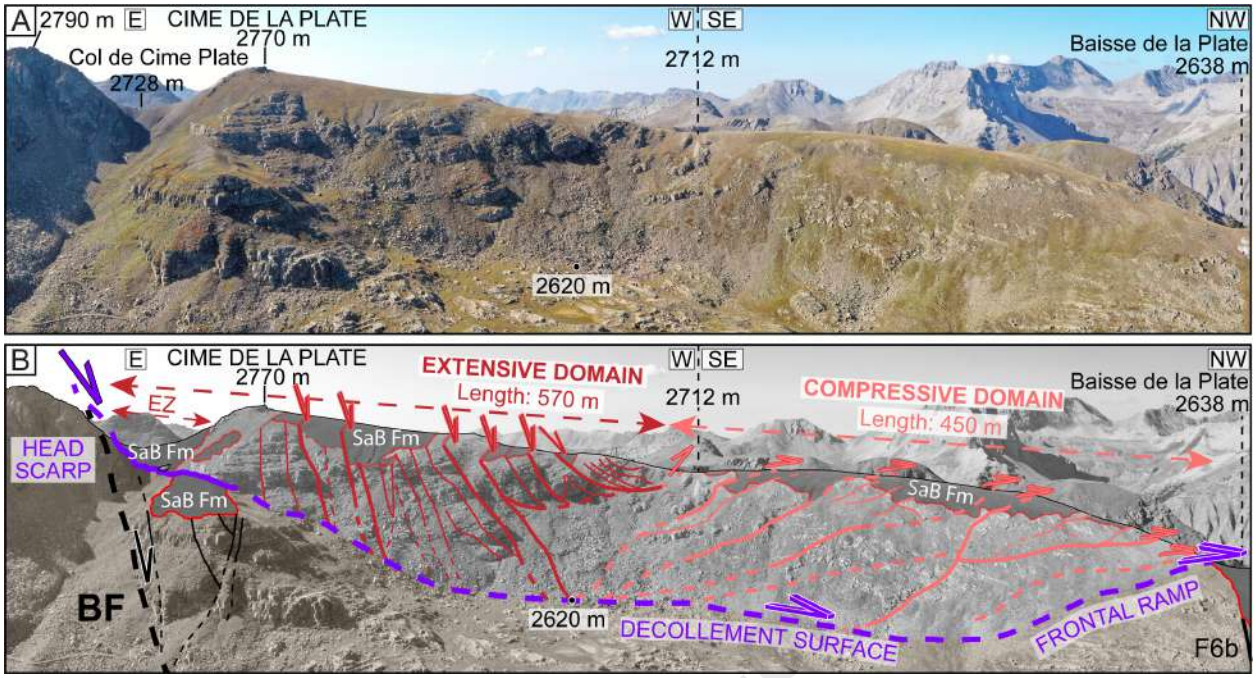

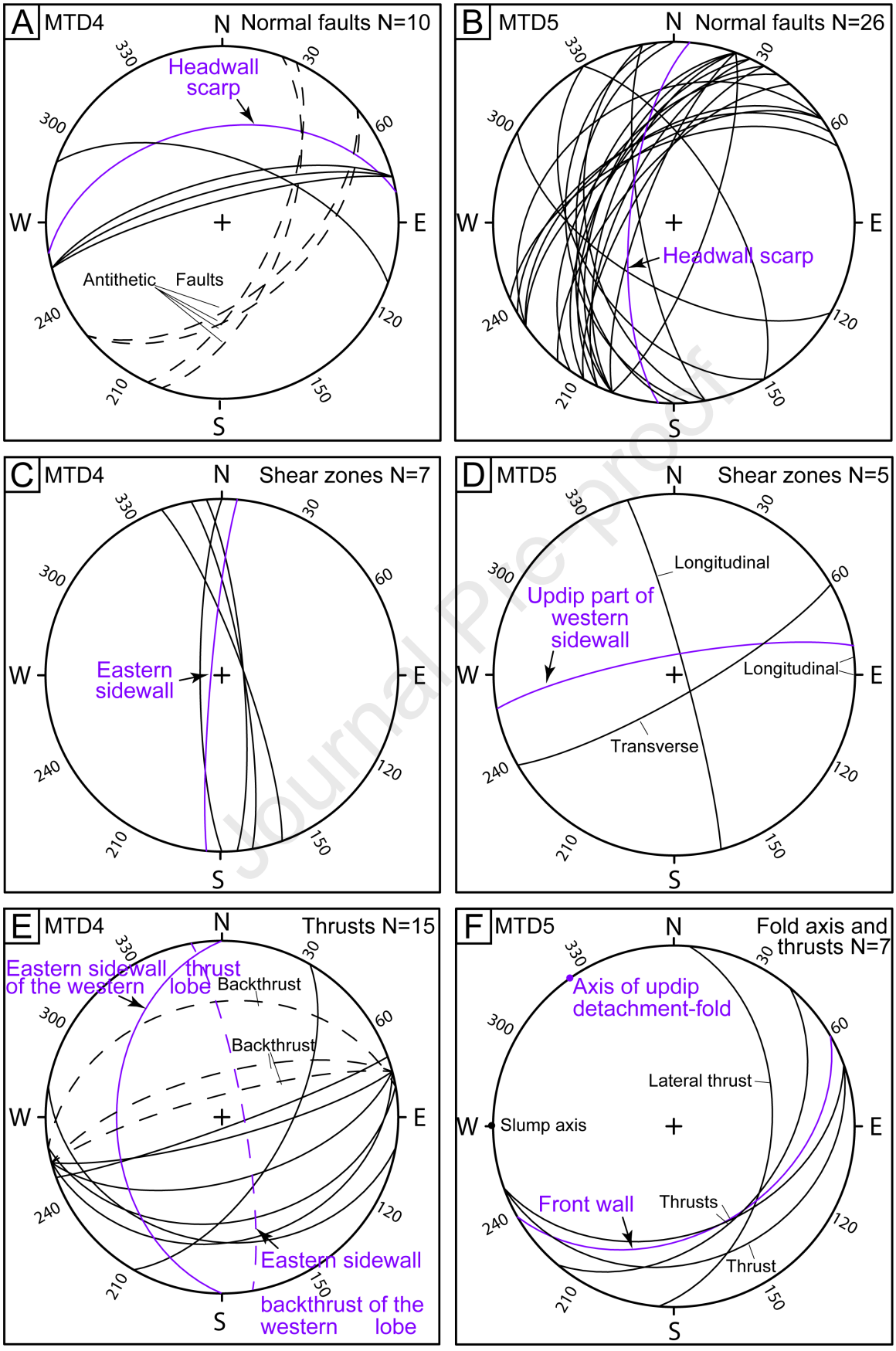
A
MTD4
N
Normal faults N=10
Headwall scarp
Antithetic Faults
B
MTD5
N
Normal faults N=26
Headwall scarp
C
MTD4
N
Shear zones N=7
Eastern sidewall
D
MTD5
N
Shear zones N=5
Longitudinal
Updip part of western sidewall
Longitudinal
Transverse
E
MTD4
N
Thrusts N=15
Eastern sidewall of the western lobe thrust
Backthrust
Backthrust
Eastern sidewall backthrust of the western lobe
F
MTD5
N
Fold axis and thrusts N=7
Axis of updip detachment-fold
Lateral thrust
Slump axis
Front wall
Thrusts
Thrust
W
E
S
30
60
120
150
210
240
300
330

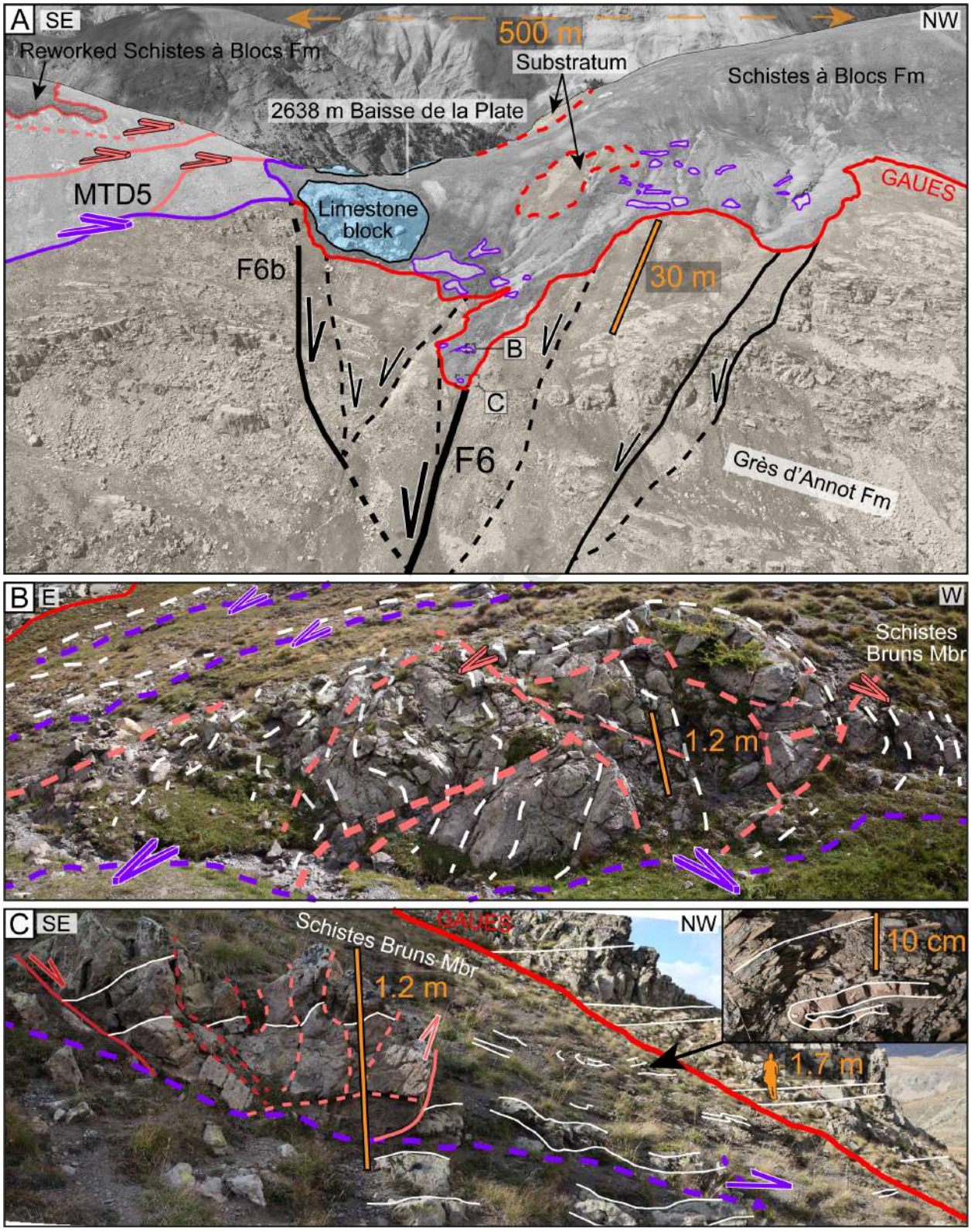
A
SE
NW
500 m
Reworked Schistes à Blocs Fm
Substratum
Schistes à Blocs Fm
2638 m Baisse de la Plate
MTD5
Limestone block
GAUES
F6b
30 m
B
C
F6
Grès d'Annot Fm
B
E
W
Schistes Bruns Mbr
1.2 m
C
SE
NW
Schistes Bruns Mbr
GAUES
1.2 m
10 cm
1.7 m

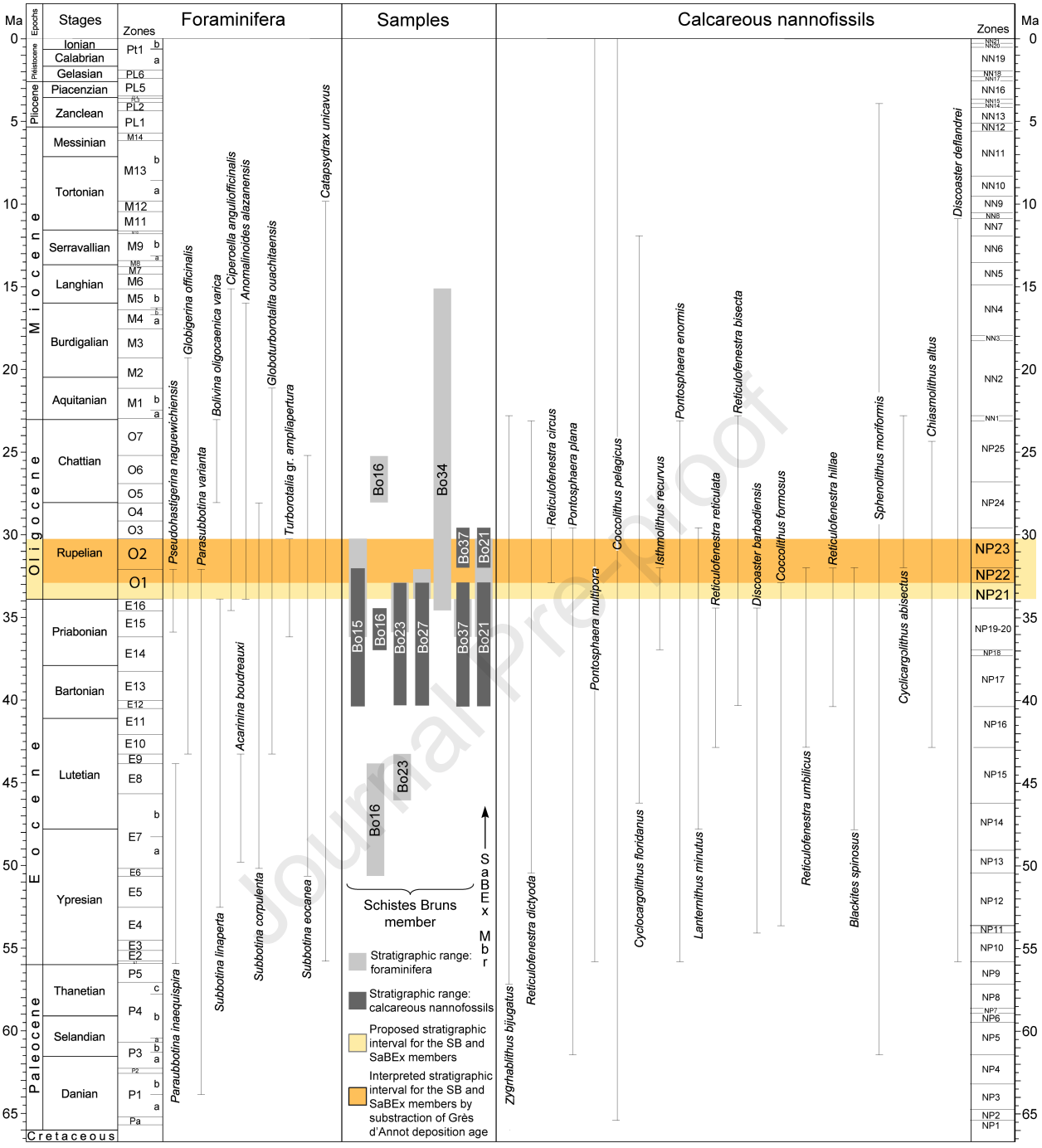

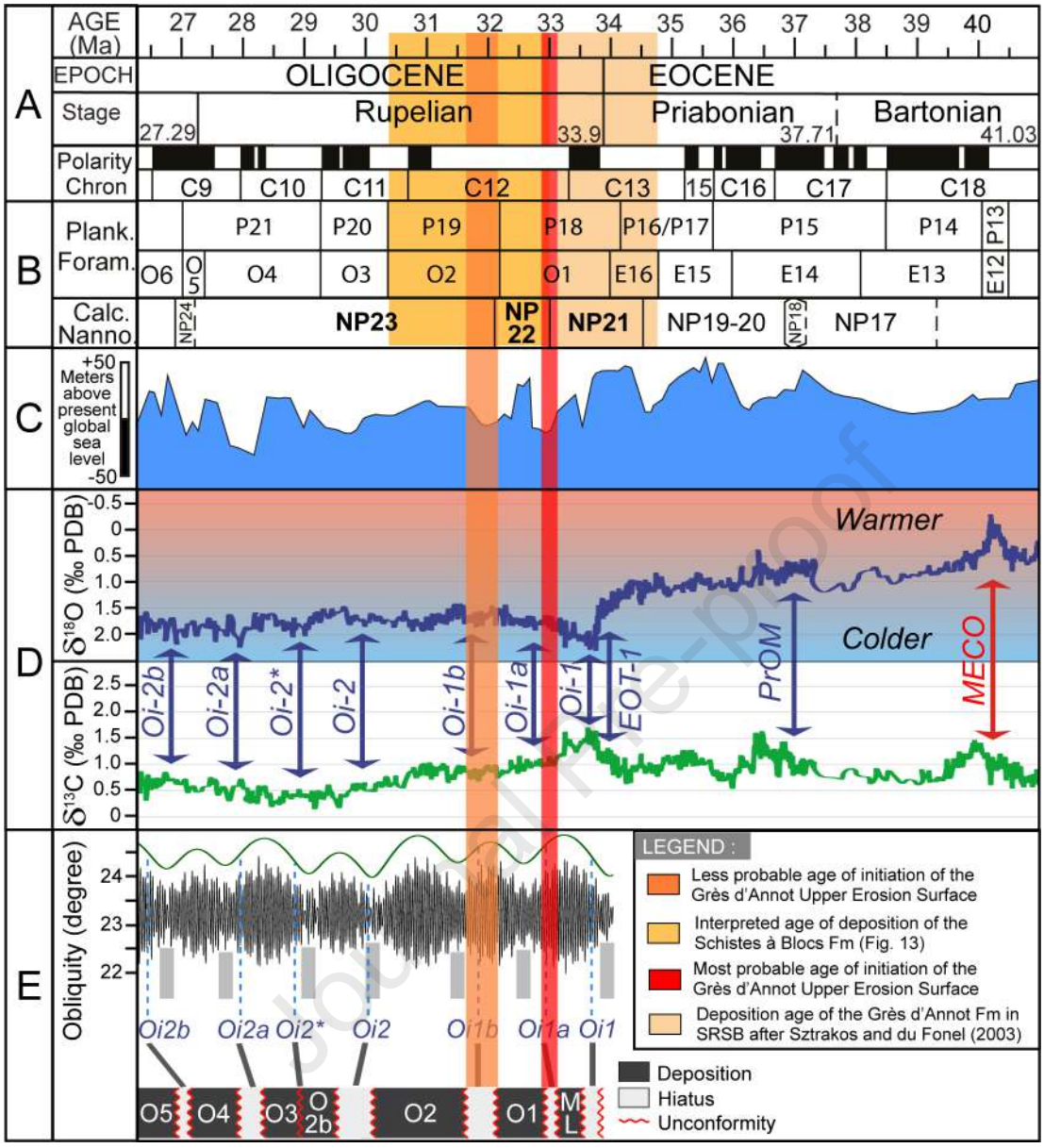
A
AGE (Ma)
27 28 29 30 31 32 33 34 35 36 37 38 39 40
EPOCH
OLIGOCENE
EOCENE
Stage
Rupelian
Priabonian
Bartonian
27.29
33.9
37.71
41.03
Polarity Chron
C9 C10 C11 C12 C13 15 C16 C17 C18
B
Plank. Foram.
P21 P20 P19 P18 P16/P17 P15 P14 P13
O6 O5 O4 O3 O2 O1 E16 E15 E14 E13 E12
Calc. Nanno.
NP24 NP23 NP 22 NP21 NP19-20 NP18 NP17
C
+50 Meters above present global sea level -50
D
δ18O (‰ PDB)
-0.5 0 0.5 1.0 1.5 2.0
Warmer
Colder
δ13C (‰ PDB)
2.5 2.0 1.5 1.0 0.5 0
Oi-2b
Oi-2a
Oi-2*
Oi-2
Oi-1b
Oi-1a
Oi-1
EOT-1
PrOM
MECO
E
Obliquity (degree)
24 23 22
Oi2b Oi2a Oi2* Oi2 Oi1b Oi1a Oi1
O5 O4 O3 O 2b O2 O1 M L
LEGEND :
Less probable age of initiation of the Grès d'Annot Upper Erosion Surface
Interpreted age of deposition of the Schistes à Blocs Fm (Fig. 13)
Most probable age of initiation of the Grès d'Annot Upper Erosion Surface
Deposition age of the Grès d'Annot Fm in SRSB after Sztrakos and du Fonel (2003)
Deposition
Hiatus
Unconformity

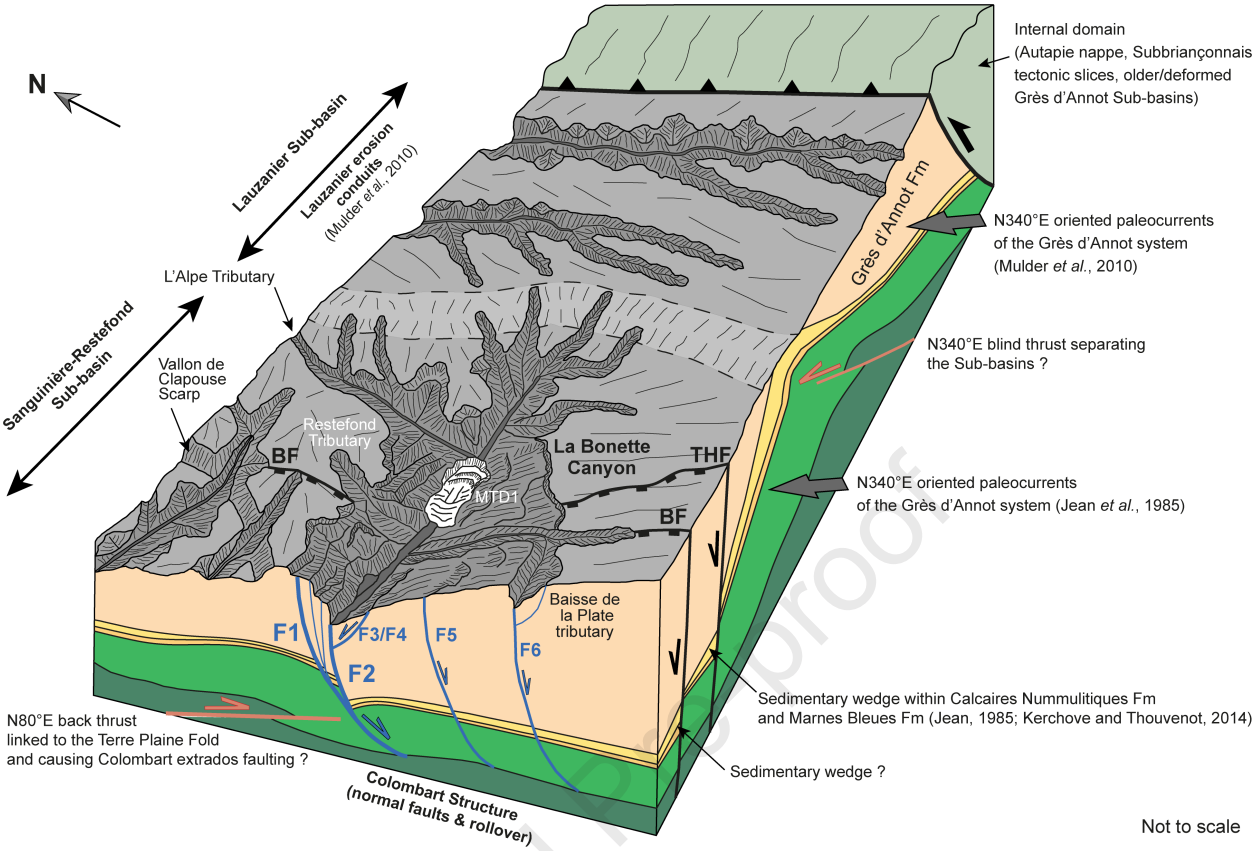

Highlights

_ Characterization of an ancient submarine canyon in an Oligocene foreland basin and reconstruction of its planform pattern by combining field observations and GIS modelling.

_ Asymmetrical cross-section profile of a submarine canyon controlled by syn-sedimentary normal faults and rollover anticline.

_ Formation of walls, ramps and terraces shaping canyon flanks by retrogressive erosion affecting partially lithified sandstones.

_ Control on location of walls, ramps and terraces by syn-sedimentary normal faults.

_ Canyon incision and retrogressive erosion both triggered by basin deformation and eustatic fall.

Declaration of interests

☐ The authors declare that they have no known competing financial interests or personal relationships that could have appeared to influence the work reported in this paper.

☒ The authors declare the following financial interests/personal relationships which may be considered as potential competing interests:

Louison Mercier reports financial support was provided by TotalEnergies SE. Louison Mercier reports financial support was provided by National Association of Technical Research.